UCRL-52827

A THREE-DIMENSIONAL CALCULATION OF THE VENTING PROCESS FOR AN ON-AXIS EXPLOSION IN THE MX TRENCH

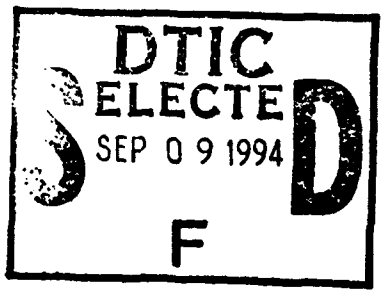

Wallace E. Johnson
Mary E. Cunningham
Louise K. Morris

September 24, 1979

Lawrence Livermore Laboratory

Work performed under the auspices of the U.S. Department of Energy by the Lawrence Livermore Laboratory under Contract W-7405-Eng-48.

UCRL-52827
Distribution Category
UC-2

A THREE-DIMENSIONAL CALCULATION OF THE VENTING PROCESS FOR AN ON-AXIS EXPLOSION IN THE MX TRENCH

Wallace E. Johnson*
Mary E. Cunningham
Louise K. Morris

Manuscript date: September 24, 1979

*Computer Code Consultants, Incorporated, Los Alamos, NM.

LAWRENCE LIVERMORE LABORATORY
University of California · Livermore, California · 94550

CONTENTS

A THREE-DIMENSIONAL CALCULATION OF THE VENTING PROCESS FOR AN ON-AXIS EXPLOSION IN THE MX TRENCH

ABSTRACT

Using the TRIDORF code, we performed a three-dimensional calculation to study the venting of energy through the roof of the proposed MX missile emplacement trench for an on-axis detonation of 1 Mt. A two-dimensional calculation to 27 μs by Science Applications, Incorporated, gave us the initial conditions; our calculation extended to 238 μs, through the period in which venting and asymmetrical tunnel expansion are the major energy-transfer processes in the trench. These two calculations provide the best available starting conditions for later 1-1/2- and 2-dimensional calculations of the downstream flow.

INTRODUCTION

One of the options considered by the Air Force for land-based weapon systems is the MX trench. To assess the degree of protection afforded the missile by blast doors and ribs in the trench walls, calculations have been made with quasi-one-dimensional and two-dimensional codes of the trench environment during an enemy attack for near-misses, direct hits, and in-trench explosions.[1-3] Because the problem is inherently three-dimensional, various leakage models have been used to simulate venting through the tunnel roof. In terms of machine size and running time, quasi-one-dimensional codes are the most practical means of carrying out calculations over long distances and to very late times. For shorter distances and shorter times, to approximate the three-dimensional configuration, two-dimensional calculations have been made along the plane of symmetry of the problem and for a cross-sectional plane through the source. However, from the onset of venting through the period in which venting is the major energy-transfer process, when the phenomenology of interest is truly three-dimensional, three-dimensional calculations are needed.

To investigate trench conditions during the restricted period in which roof venting is expected to be the dominant transfer mechanism, we performed a three-dimensional calculation using the TRIDORF version of W. E. Johnson's TRIOIL code. TRIDORF,[4] a two-material, three-dimensional, Eulerian hydrodynamic code, has a rigid-plastic strength model and radiation diffusion capability. The calculation run as a purely hydrodynamic problem extended from about 27 μs, when the problem is just becoming three-dimensional, to about 260 μs. This report describes the code and calculational setup, gives results of our calculations to 238 μs, and compares our results at 260 μs with those of quasi-one-dimensional and two-dimensional calculations.

CODE AND CALCULATIONAL SETUP

The original problem involved a 1-Mt source detonated on the axis of a tunnel 4.2 m in diameter. The tunnel walls were assumed to be iron-fiber-filled concrete 0.275 m thick. The surrounding medium was alluvium and the overburden thickness 1.495 m.

We generated the three-dimensional problem by linking to a two-dimensional calculation performed by SAI (Science Applications, Incorporated) using the DRAGNET and RADOIL codes. The link was made at 27.06 μs, when the problem was still two-dimensional. The TRIDORF

generator spun the two-dimensional problem about its axis to form half the cylindrical tunnel and also added air above the tunnel and more alluvium below, forming the three-dimensional problem illustrated in Fig. 1.

Figures 2 through 4 show the zoning for the TRIDORF problem along with the corresponding material maps at link time. In all, the calculation used 36,000 zones: 30 zones (JMAX) covering 87.37 m from the source along the tunnel length, 50 zones (IMAX) extending 41.18 m in the direction perpendicular to both the tunnel axis and the ground surface, and 24 zones (KMAX) extending 8.44 m in the third direction. The two-dimensional RADOIL problem to which TRIDORF was linked had 61 zones along the tunnel axis and 137 in the radial direction. Because of storage limitations in the CDC 7600 computer, the full length of the tunnel in the RADOIL problem was not included in the TRIDORF calculation but only the 87 m (55 of 61 zones) needed to carry it past the time when venting is expected to dominate. Large "sink" zones were placed at the edges of the problem except at the plane of symmetry and the tunnel ends. To allow a better resolved calculation of the venting, more zones were used on the external-air side of the problem above the trench than below it. Transmittive boundary conditions allowing the passage of momentum and energy over the grid boundaries were applied except across the plane of symmetry.

To maintain consistency with the two-dimensional SAI calculation, the equations of state in TRIDORF were made identical with those in their version of RADOIL. Because both are intrinsically two-material codes, the tunnel wall material and tunnel air were labeled as one material (dot) distinguished only by density. When the density of the dot material was less than 0.005 g/cm^3, it was treated as air and described as an ideal gas with a γ of 1.5. For greater densities it was treated as concrete using a modified form of the Tillotson equation. The constants for the concrete are given in Table I along with those for the alluvium (X material) outside the trench wall.

The modified Tillotson equation of state for the dot and X materials was as follows. Let ρ_0 be the normal density, ρ the density of the material in the zone, P the pressure, and I the specific internal energy. The constant A is the bulk modulus; G is the zero-pressure Grüneisen constant. I_0, b, B, α, and β are fitting constants. The quantity I_s is the specific internal energy of the material at the

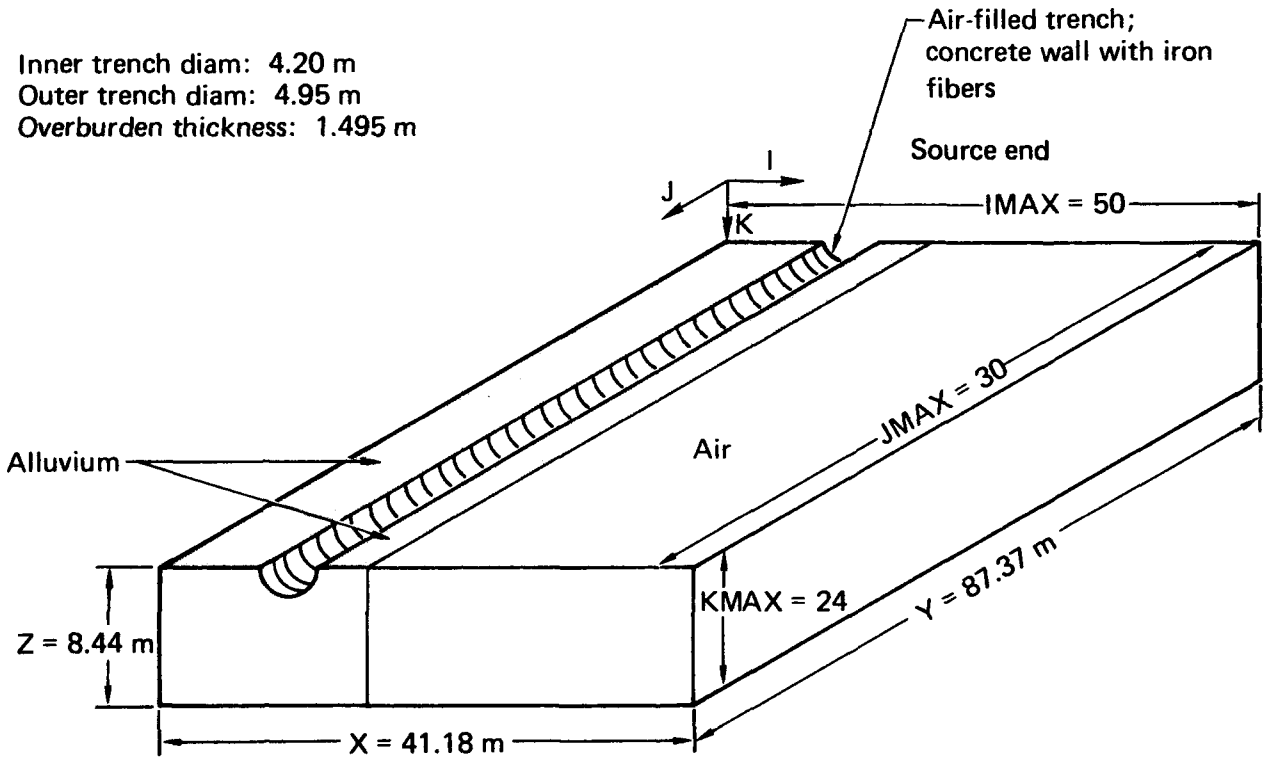

FIG. 1. MX configuration at three-dimensional link time (27 μs).

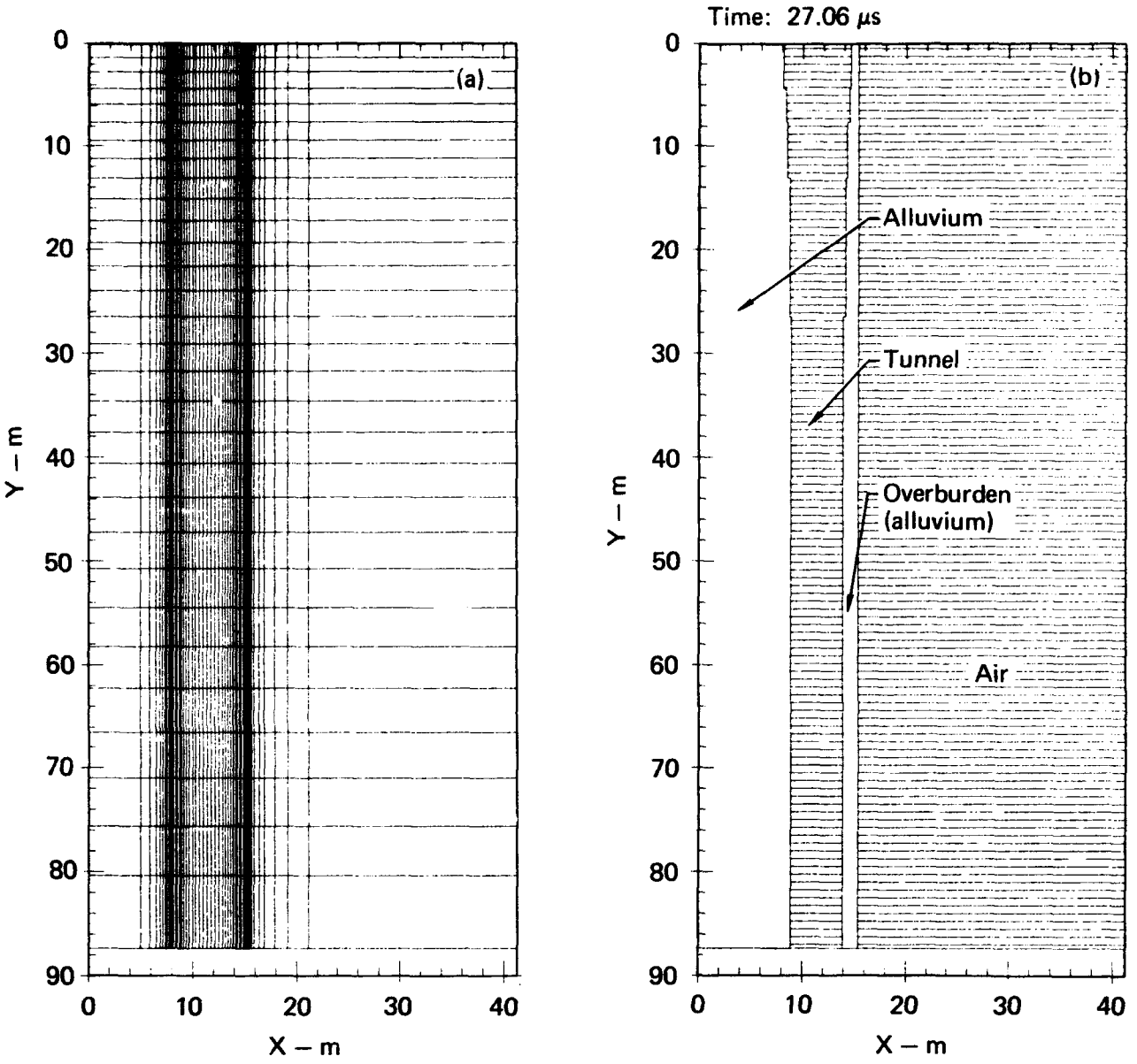

FIG. 2. Symmetry plane: (a) X-Y zoning; (b) material map.

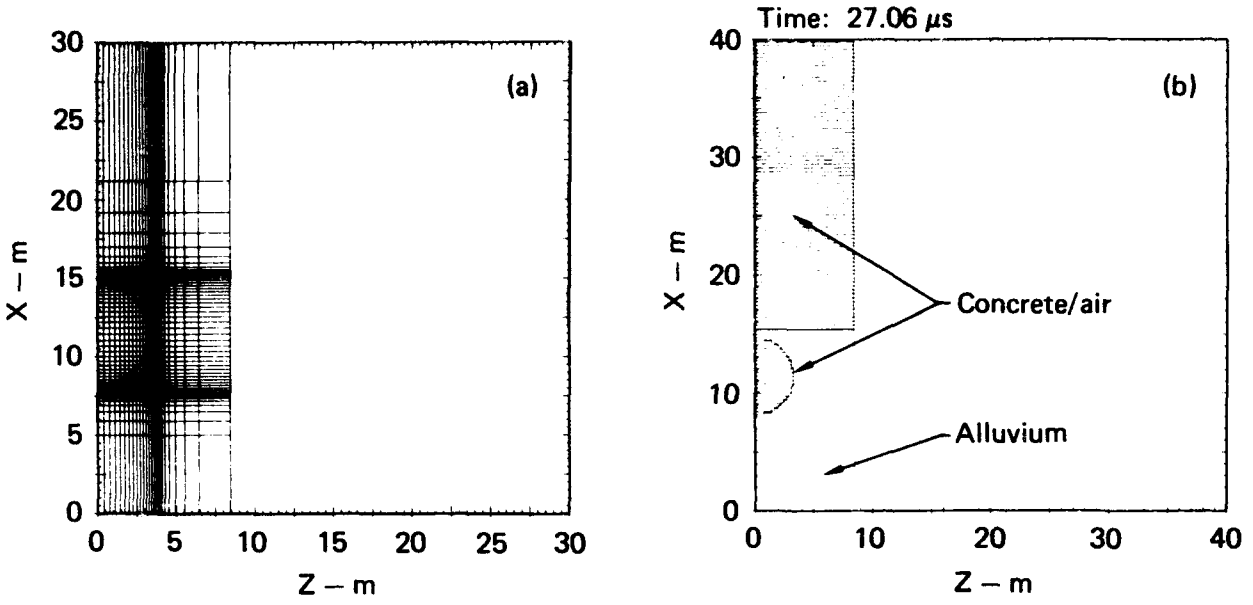

FIG. 3. Cross-sectional plane: (a) Z-X zoning; (b) material map.

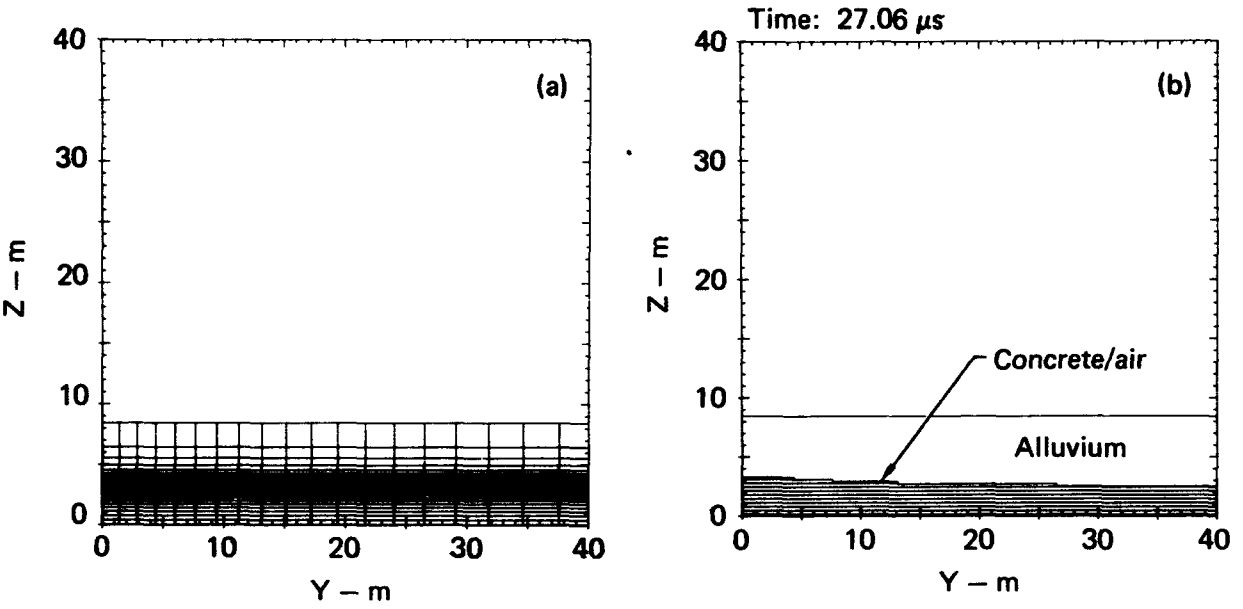

FIG. 4. Longitudinal plane: (a) Y-Z zoning; (b) material map for 40-m area closest to source.

vaporization temperature; I_s' is equal to I_s plus the energy needed to vaporize the material from the liquid state. Thus:

$$\eta = \rho/\rho_0$$

$$\mu = \rho/\rho_0 - 1$$

$$G = \left(a + \frac{b}{\left[I/\left(I_0\eta^2\right)\right] + 1}\right)$$

For $\eta \geq 1$:

$$P(\rho, I) = G\rho I + A\mu + B\mu^2$$

For $\eta < 1$ and $I \leq I_s$:

$$P_a(\rho, I) = G\rho I + A\mu$$

For $\eta < 1$ and $I \geq I_s'$:

$$P_b(\rho, I) = aI\rho + \left(\frac{bI\rho}{\left[I/\left(I_0\eta^2\right)\right] + 1} + A\mu e^{-\alpha[(\rho_0/\rho) - 1]}\right) e^{-\beta[(\rho_0/\rho) - 1]^2}$$

For $\eta < 1$ and $I_s < I < I_s'$:

$$P(\rho, I) = \left(\frac{I_s' - I}{I_s' - I_s}\right) P_b(\rho, I) + \left(\frac{I - I_s}{I_s' - I_s}\right) P_a(\rho, I)$$

TABLE 1. Tillotson constants for concrete and alluvium.

Constant	Concrete	Alluvium
ρ_0, g/cm^3	2.5	1.76
a	0.5	0.5
E_0, kJ/g	11.0	0.00201
b	1.3	1.3
A, kJ/cm^3	4.6	23.4
E_s, kJ/g	1.91	3.50
E_v, kJ/g	3.20	18.0
α	5.0	5.0
β	5.0	5.0
B, kJ/g	23.5	10.2

For concrete vapor of density less than 5×10^{-3}, a gamma-law equation of state for air was used with $(\gamma - 1) = 0.5$.

The total energy in the problem at link time (27 μs) was 1.025×10^{15} J (0.25 Mt), representing the quarter of the total 1-Mt yield that was included in the grid (see geometry in Fig. 1). At 175 μs after detonation, 1% of the total energy had flowed over the grid boundary. At 250 μs, the end of the calculation, the loss had increased to 5.8% of the total energy. The maximum amount of radiation energy in any zone at link time was about 2% of the total internal energy in that zone; hence, the radiation option in the TRIDORF code was not used. The calculation from 27 to 250 μs required some 2 h of CDC 7600 computer time.

CALCULATIONAL RESULTS TO 238 μs

Supporting the following description are plots of variables made with the TENPLT code[5] at and after link time. The calculational data allow detailed analysis of conditions in the trench during the time in which venting and asymmetrical tunnel expansion are the major energy-transfer mechanisms.

Figure 5 is a vector plot of velocities at link time. The apparent rotation of the vectors back toward the tunnel axis in the region Y = 40 m occurs because the vectors are plotted at locations along straight lines parallel to the problem axis rather than along isovelocity lines. Figure 6 is an isometric plot of the tunnel pressure at link time. The pressure front traveling radially has not yet broken through the alluvium overburden into the air. The accompanying geometrical view serves merely to orient the reader, and no distinction is made between the wall material and the alluvium. The shaded portion includes both.

Figure 7 shows plots of the pressure profile along the tunnel axis at several times during the calculation. Figure 8 is a semilog plot of these pressure profiles for the range beyond 30 m. Here one can see at about 60 m the diffusion front established at early times in the two-dimensional calculation, which was able to move no farther

down the tunnel because the coupling of most of its energy into the wall left little radiant energy to drive it. By about 80 μs this front has collapsed and has been overtaken by hydrodynamic pressure moving down the tunnel. Figure 9 shows the density profile along the tunnel axis at 28.7 μs and at 238 μs. The location of the diffusion front is again apparent in the density plot at the earlier time.

Figure 10 shows the magnitudes of the Y-directed velocities along the tunnel at the axis. Figure 11 is the material map at 238 μs. The venting process is very apparent here. Figure 12 is a blowup of the material plot in the region of the venting showing velocity vectors in that region. The vector arrows are not intended to show velocity magnitudes but indicate the direction and location of the stagnation region at the trench bottom. (Single-headed arrows are velocities larger than the scale maximum.) Similar material and velocity vectors are shown in Fig. 13 for the tunnel region beyond 40 m from the source.

Figures 14 through 17 show isometric plots of density and pressure, along with corresponding geometrical views. By 238 μs the trench top has been unzipped to about 30 m. This is also the approximate location of the pressure peak along the tunnel axis at this time, as can be seen in Fig. 18. Figures 19 through 22 show the pressure profiles along vertical lines through the tunnel axis from the trench bottom up through the overburden at increasing distances down the tunnel. At 238 μs the problem is still two-dimensional beyond 50 m. Figures 23 through 34 are cross-sectional material maps, vector velocity plots, and isometric plots of density and pressure for distances of 0.7, 28, and 50 m from the source. Figure 35 shows the trench configuration on the symmetry plane of the problem at 238 μs. Tunnel explosion has extended out to about 46 m from the source, but there is still material of significant density (greater than 1 g/cm^3) in the overburden back to about 29 m. The wall vapor-air interface as defined by the boundary density of 0.005 g/cm^3 has moved down the tunnel to about 60 m.

We calculated the fraction of total energy remaining in the original tunnel volume using the post-processer code SAMPLER.[6] Values as a function of time are shown in Fig. 36. The most rapid loss at early times results from radiant coupling of the energy to the wall, leading to rapid venting while the radiation front remains stationary in the tunnel. Venting slows as the hydrodynamic pressure front moves down the tunnel and overtakes the stagnant radiation front, producing the knee in the curve at about 60–70 μs. Venting due to the hydrodynamic pressure continues at a slower rate; at 260 μs, about 9% of the total energy remains in the original trench volume.

COMPARISON WITH ONE- AND TWO-DIMENSIONAL CALCULATIONS

SAI had performed a two-dimensional calculation in the symmetry plane of the three-dimensional TRIDORF calculation and also in the cross-sectional plane through the source.[7] Figure 37 compares peak pressures as a function of time for these calculations. At 40 μs stagnation occurs on-axis, producing a peak in the profile. In a two-dimensional code this pressure should be better calculated in transverse than in longitudinal geometry and, indeed, we find excellent agreement between the transverse two-dimensional and TRIDORF calculations. In general, the peak pressures by TRIDORF are 30-35% lower than by the two-dimensional calculations. This is to be expected because the three-dimensional calculation has the additional divergence term. The two-dimensional calculations are thus somewhat conservative. Figures 38 through 40, showing density, pressure, and velocity profiles at 260 μs, also exhibit this tendency.

Figure 41 shows pressure vs distance down the tunnel. Comparison is made between the SAI quasi-one-dimensional (STEALTH) calculation and the on-axis values for the TRIDORF calculation at 250 μs. The peak pressure has advanced about 100 m farther downstream in the one-dimensional calculation than in the three-dimensional calculation, but the values of peak pressure for the two calculations are almost identical at 250 μs. Different venting models might be tried for the one-dimensional calculation to reduce the discrepancy. This would be worthwhile because the one-dimensional calculation is the only practical one to pursue at very late times.

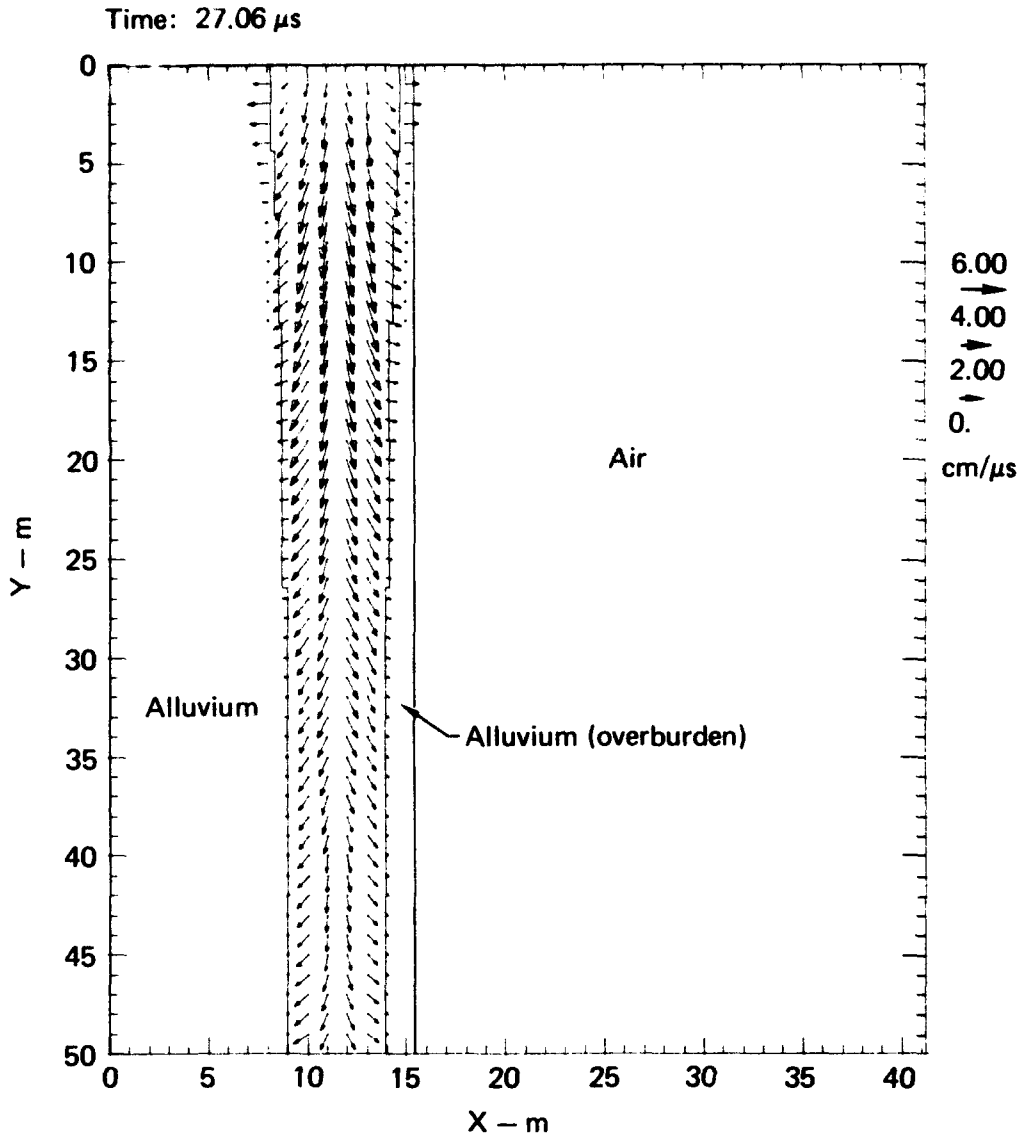

FIG. 5. Velocities on symmetry plane at link time.

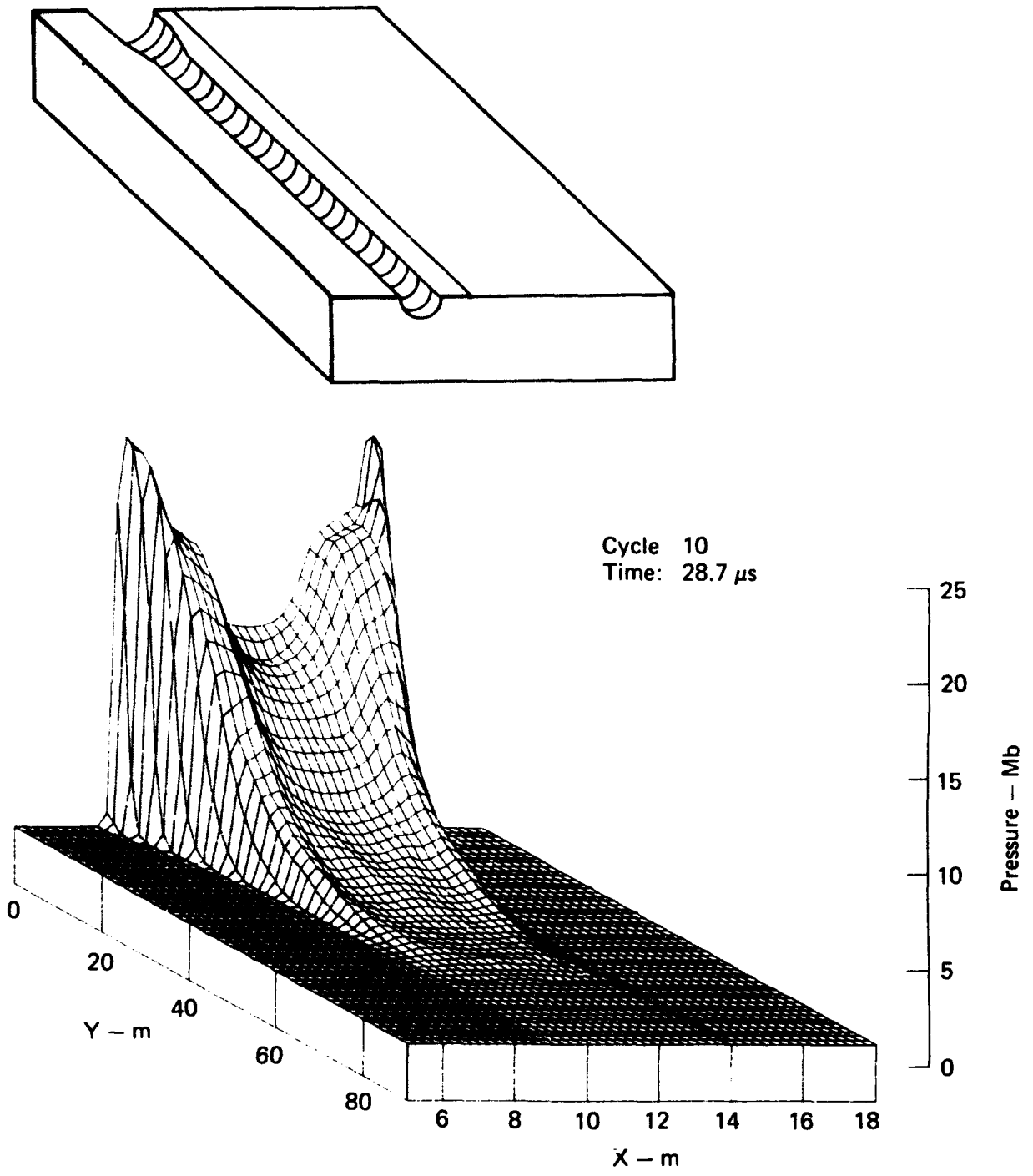

FIG. 6. Pressure isometric plot at link time.

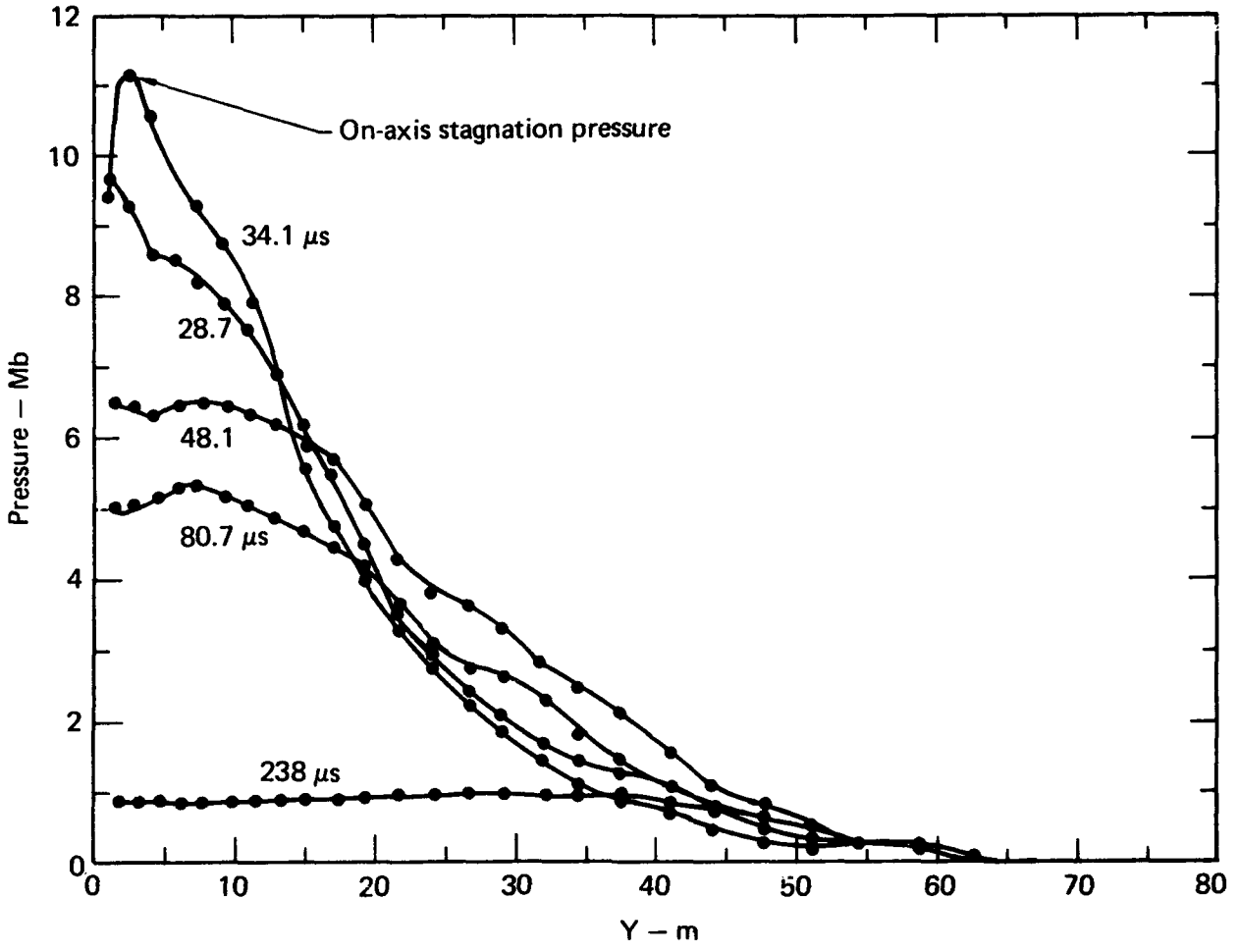

FIG. 7. Pressure along tunnel axis.

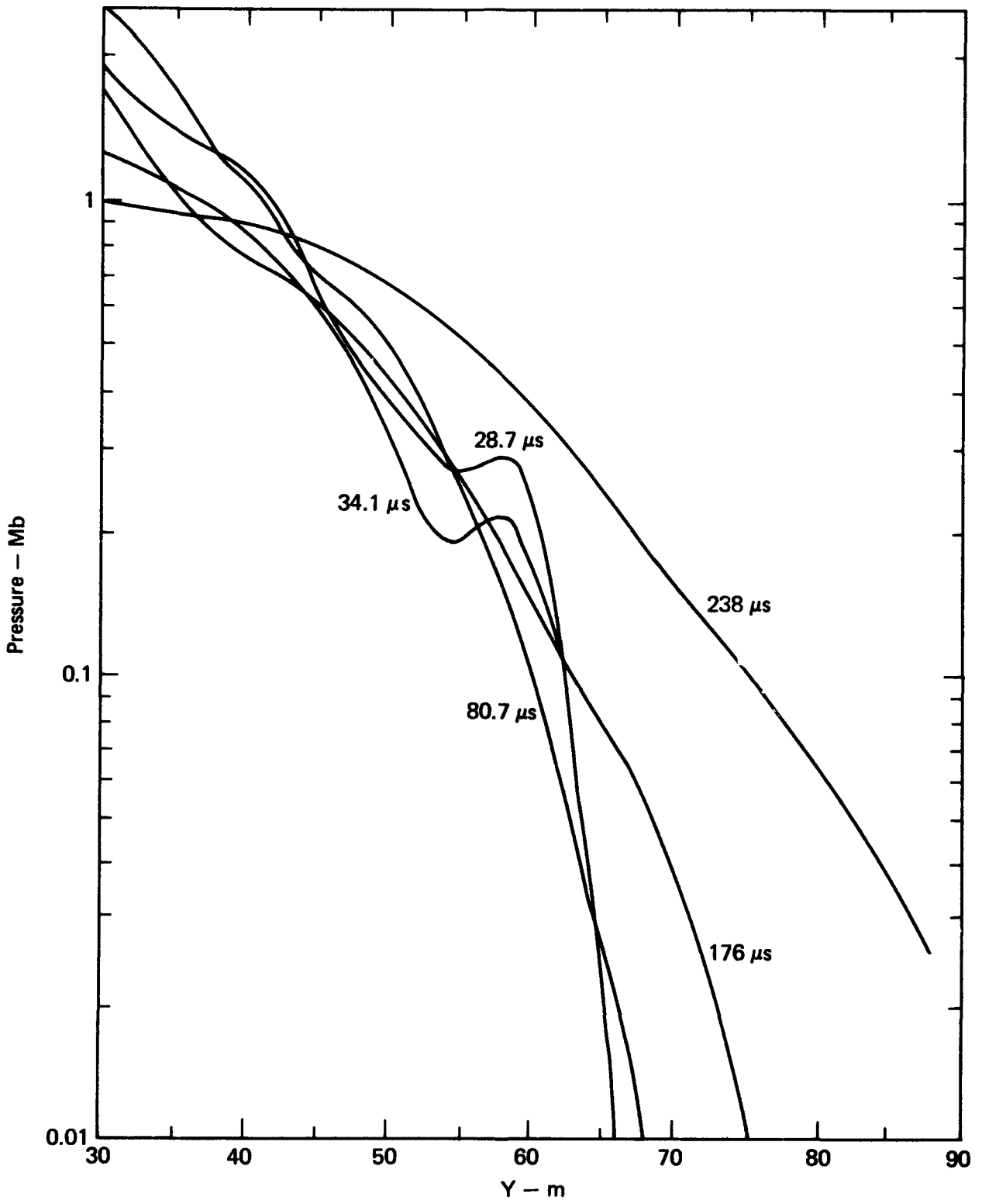

FIG. 8. Detail of pressure front along tunnel axis.

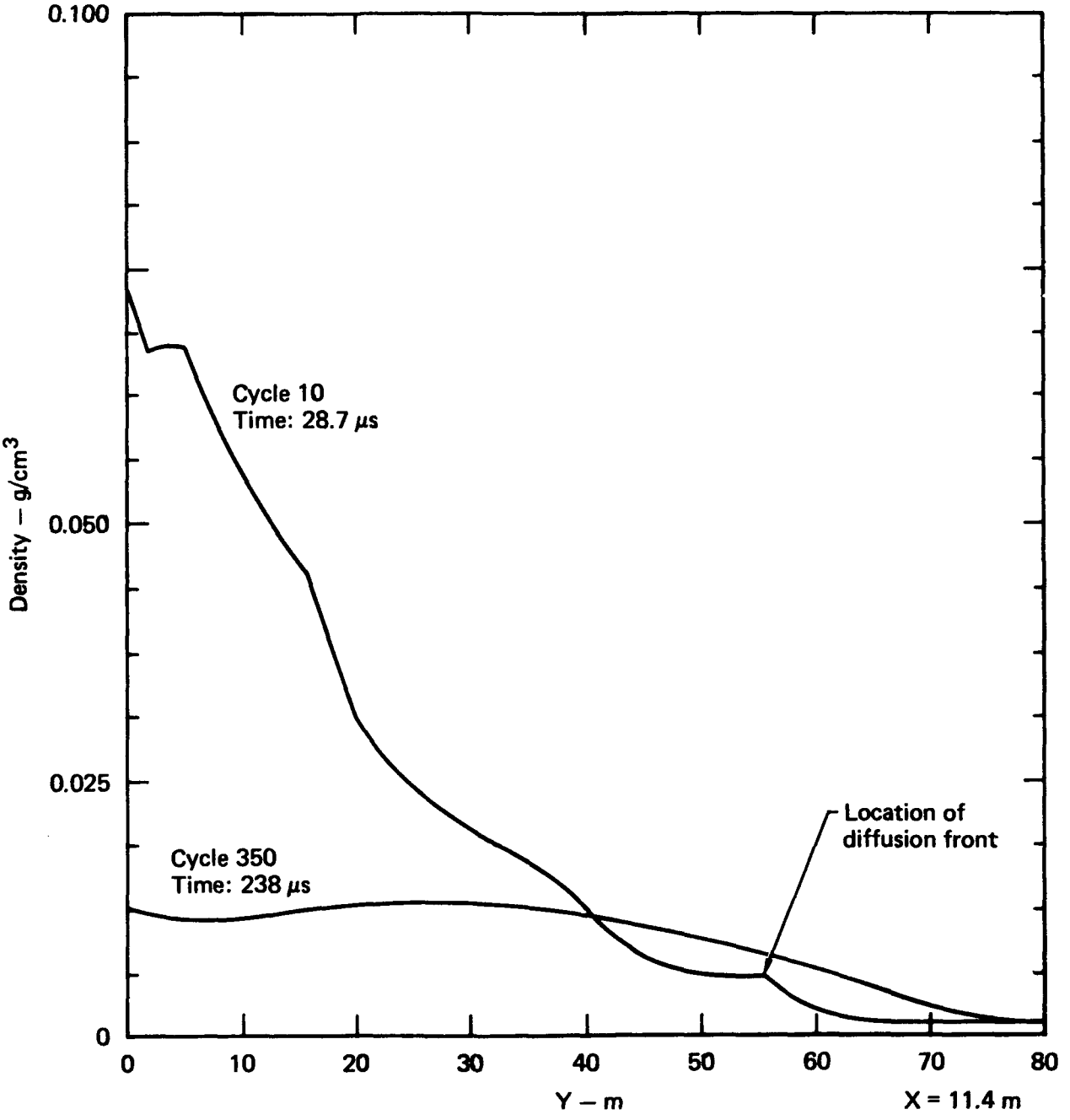

FIG. 9. Density profile along tunnel axis.

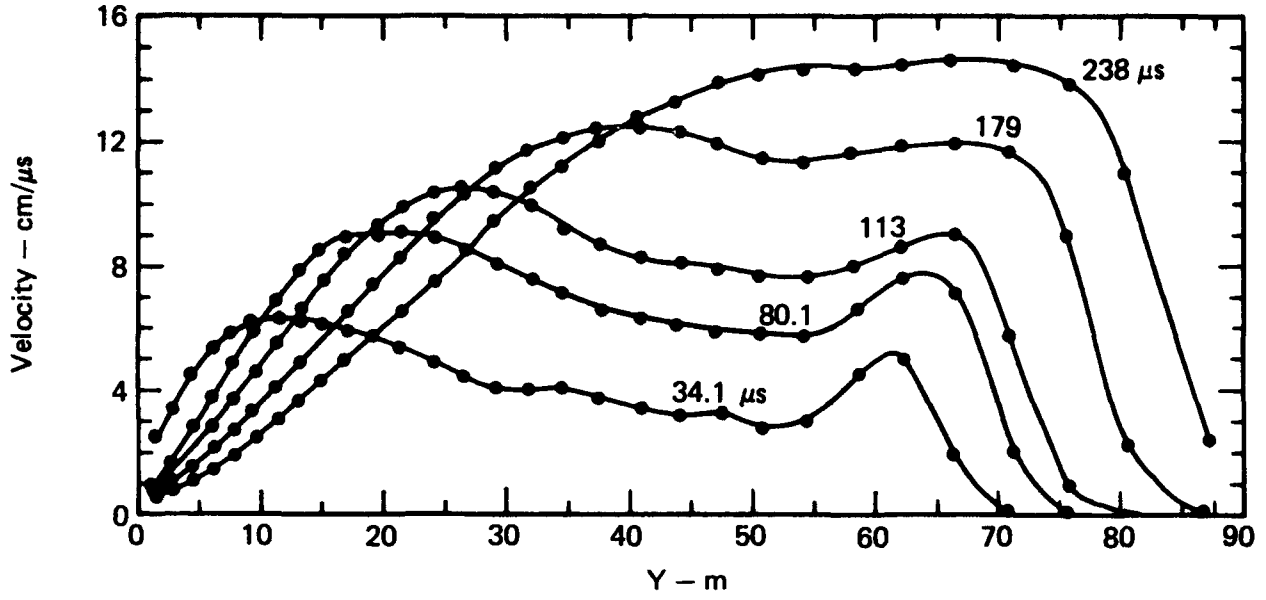

FIG. 10. Magnitude of velocity in Y direction along tunnel axis.

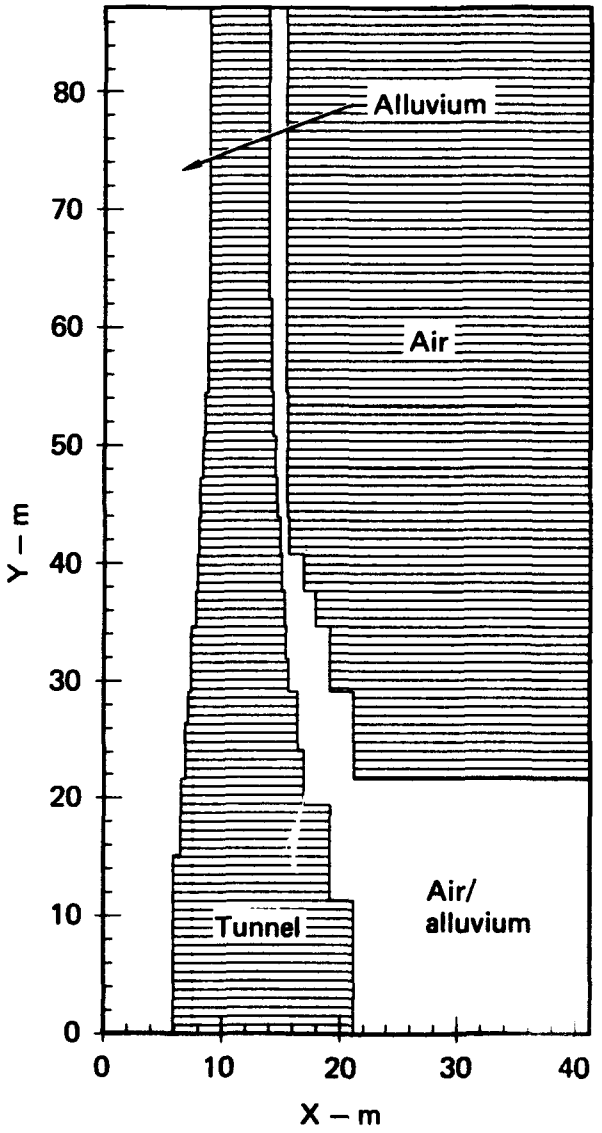

FIG. 11. Material plot on symmetry plane at 238 μs.

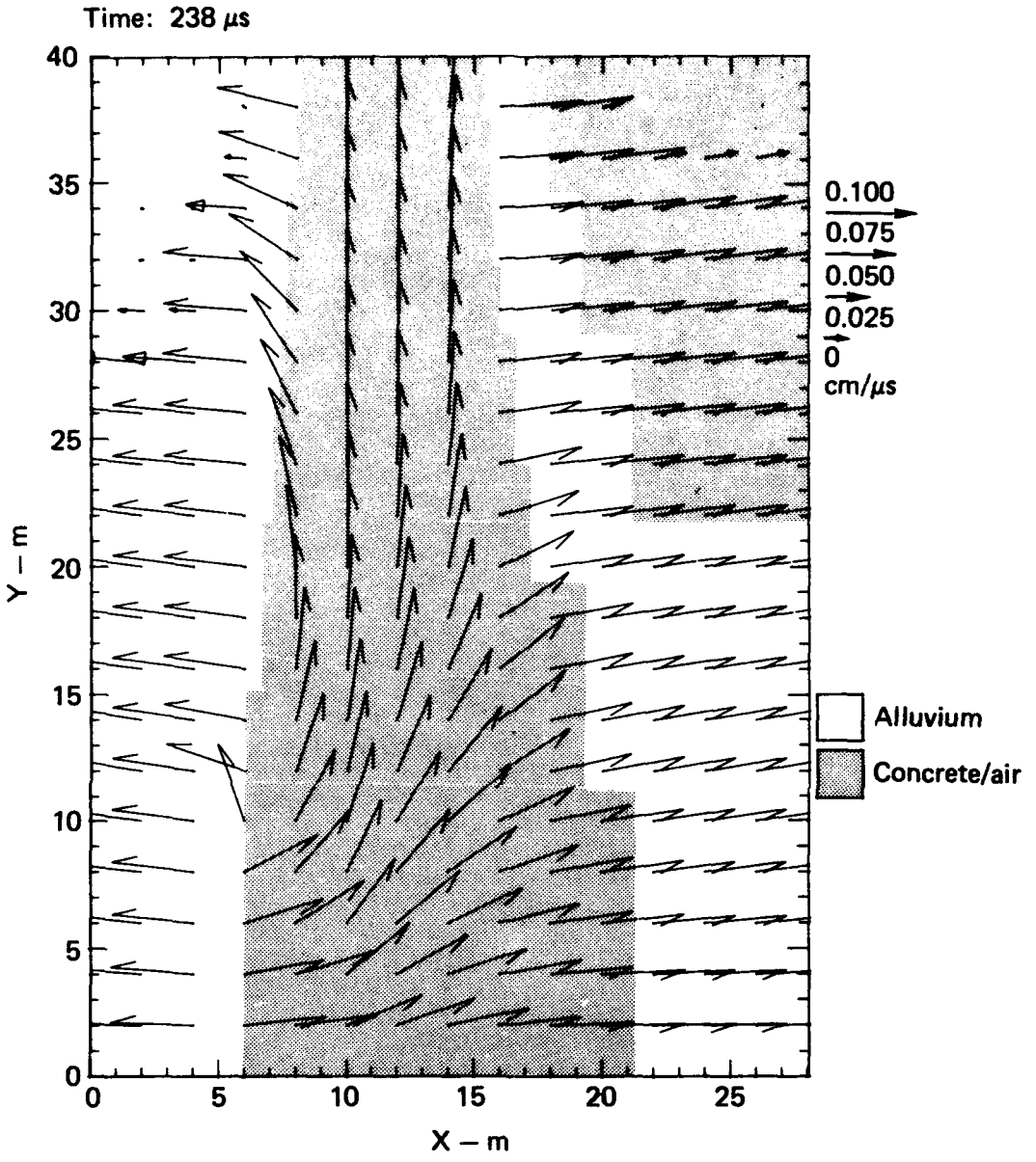

FIG. 12. Expanded material plot with velocity vectors on symmetry plane at 238 μs (source end).

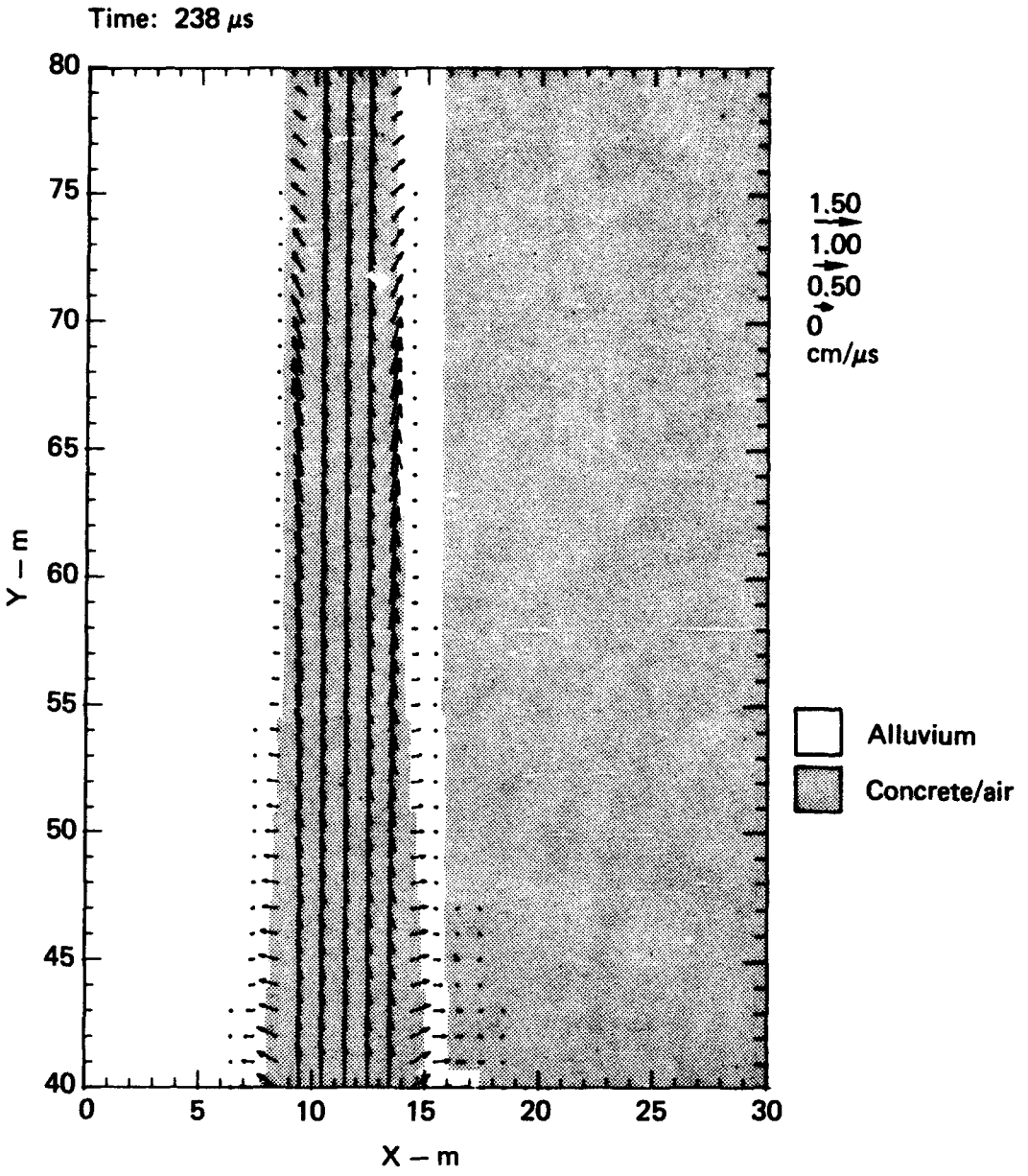

FIG. 13. Expanded material plot with velocity vectors on symmetry plane at 238 μs (downstream end).

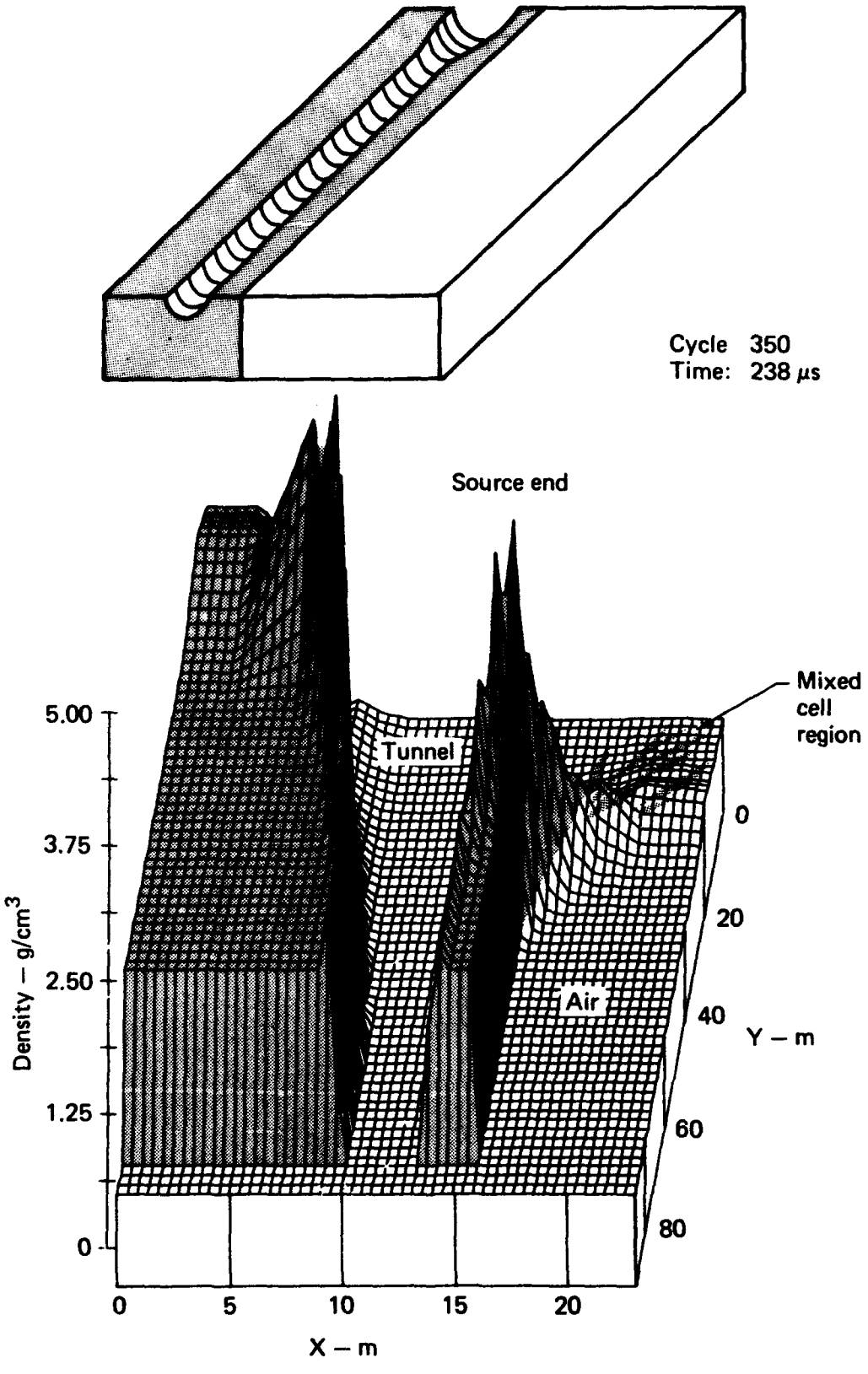

FIG. 14. Isometric plot of density on symmetry plane at 238 μs (looking from downstream end).

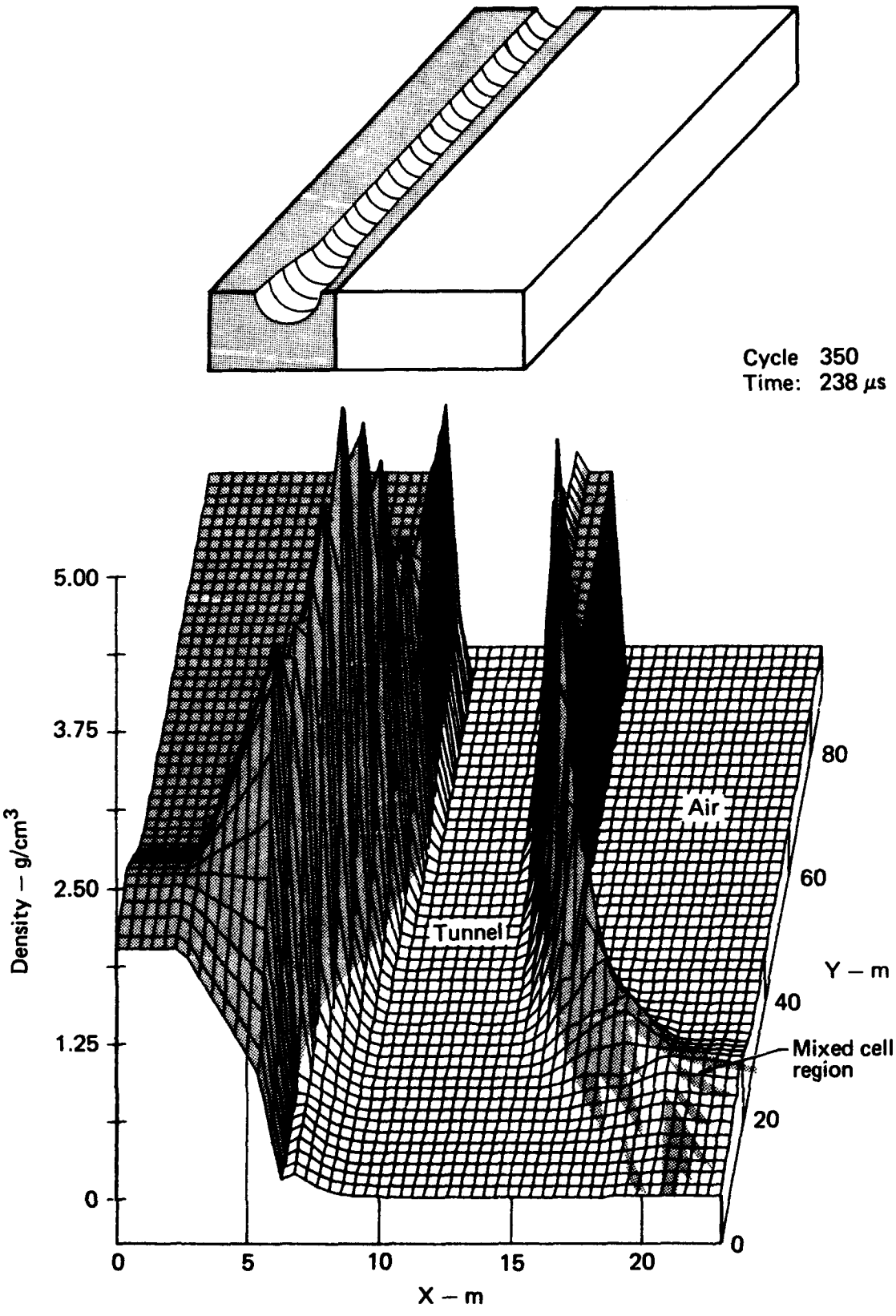

FIG. 15. Isometric plot of density on symmetry plane at 238 μs (looking from source end).

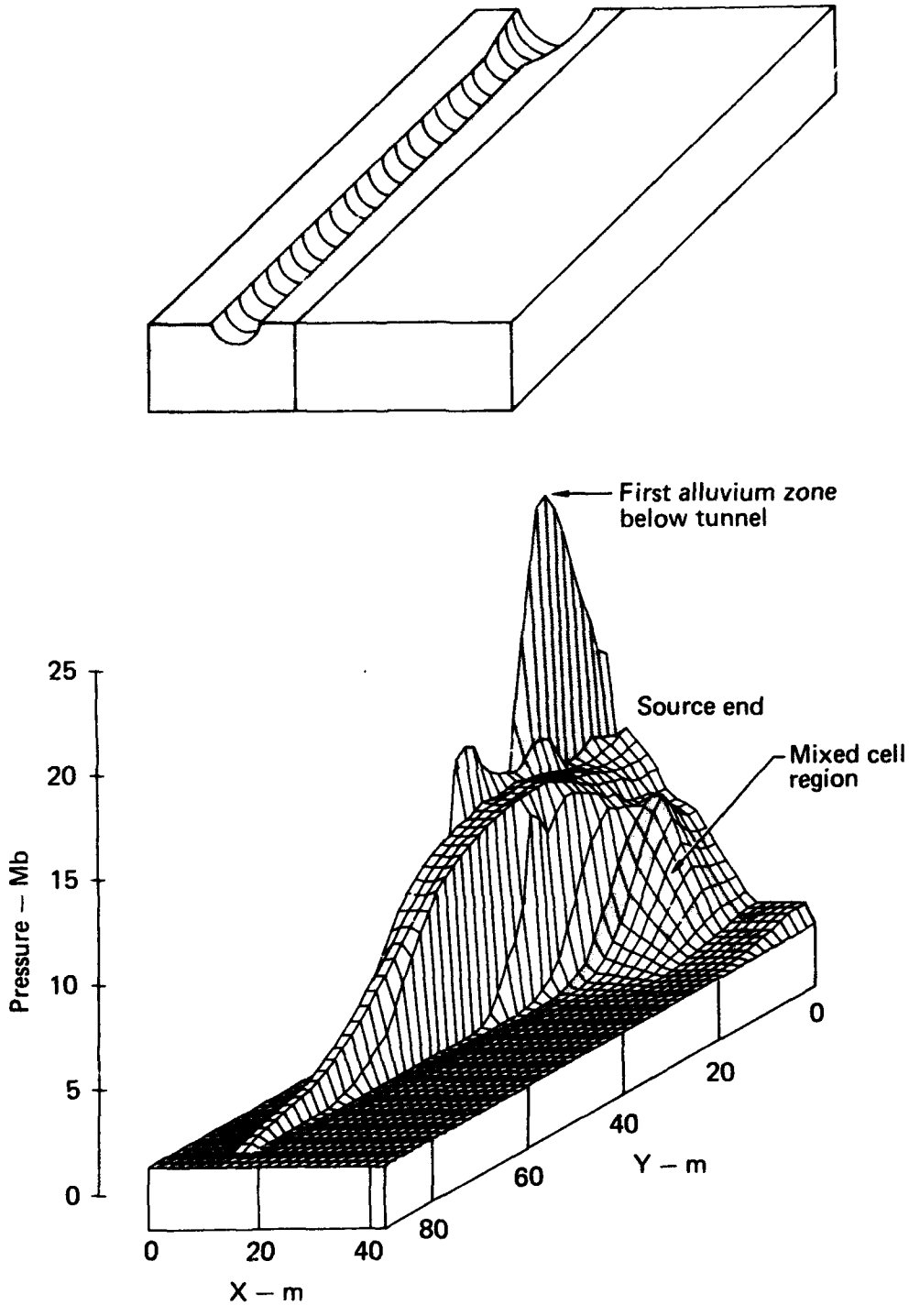

FIG. 16. Isometric plot of pressure on symmetry plane at 238 μs (looking from downstream end).

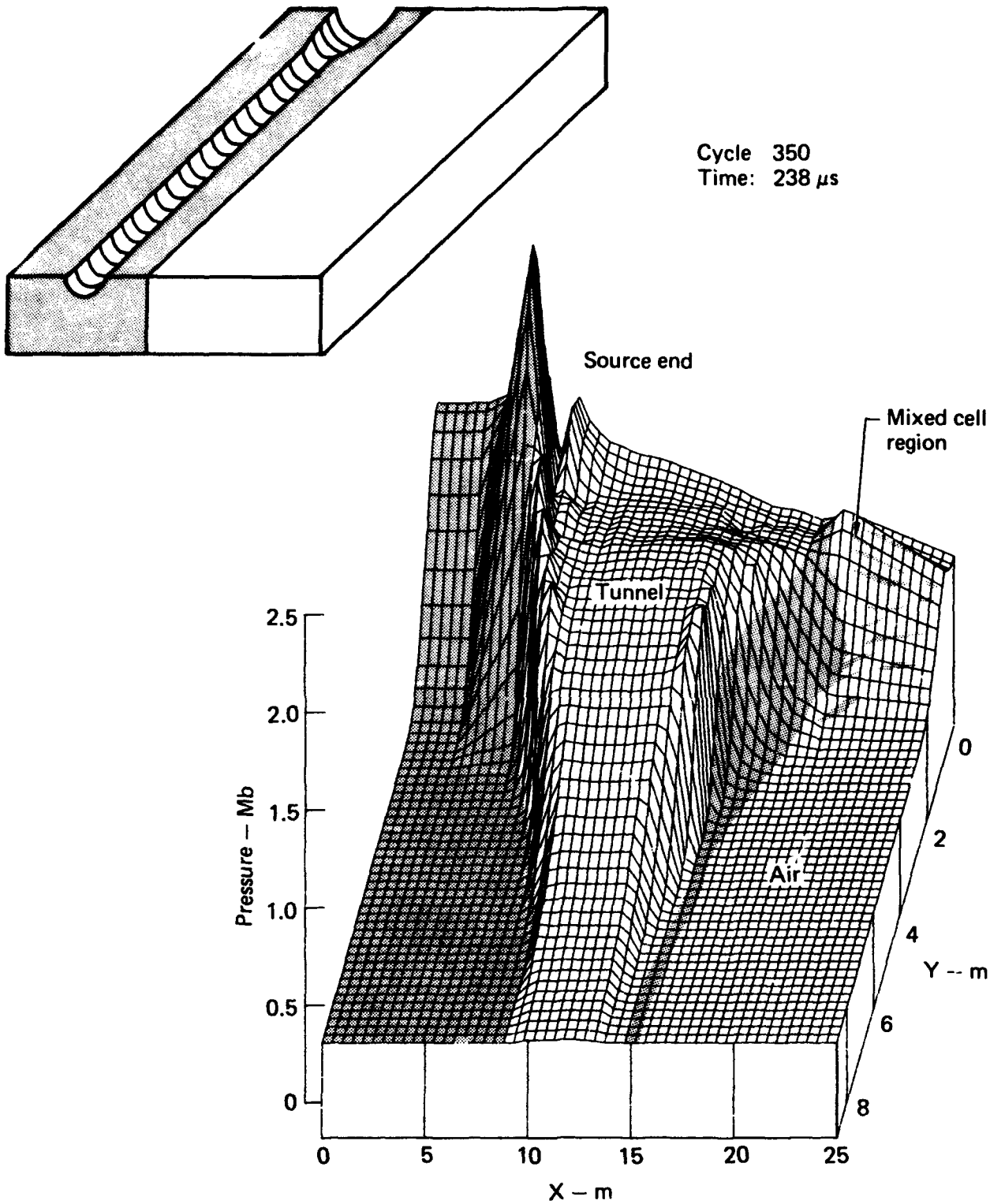

FIG. 17. Isometric plot of pressure on symmetry plane at 238 μs (looking from downstream end).

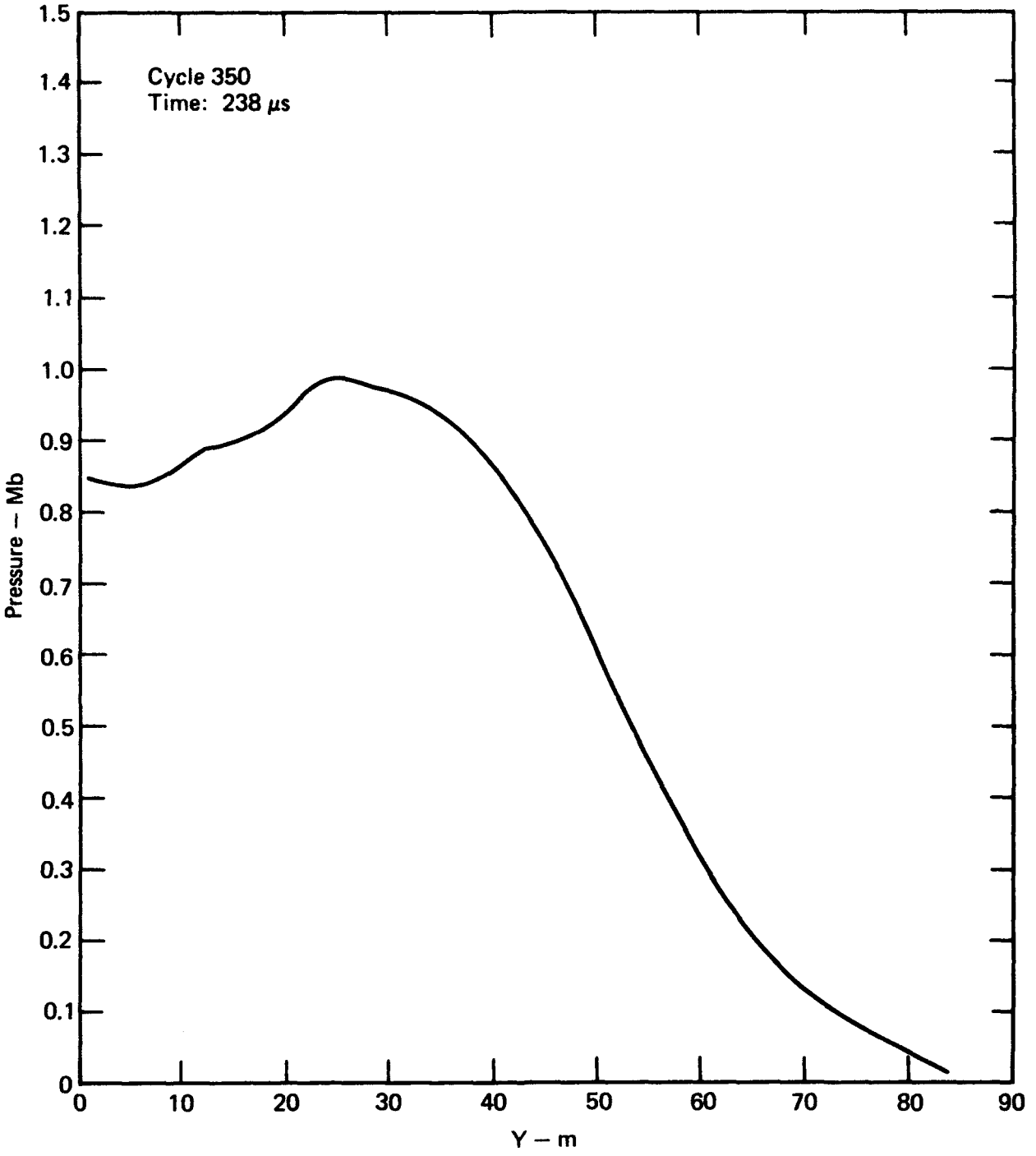

FIG. 18. Pressure profile along tunnel axis at 238 μs.

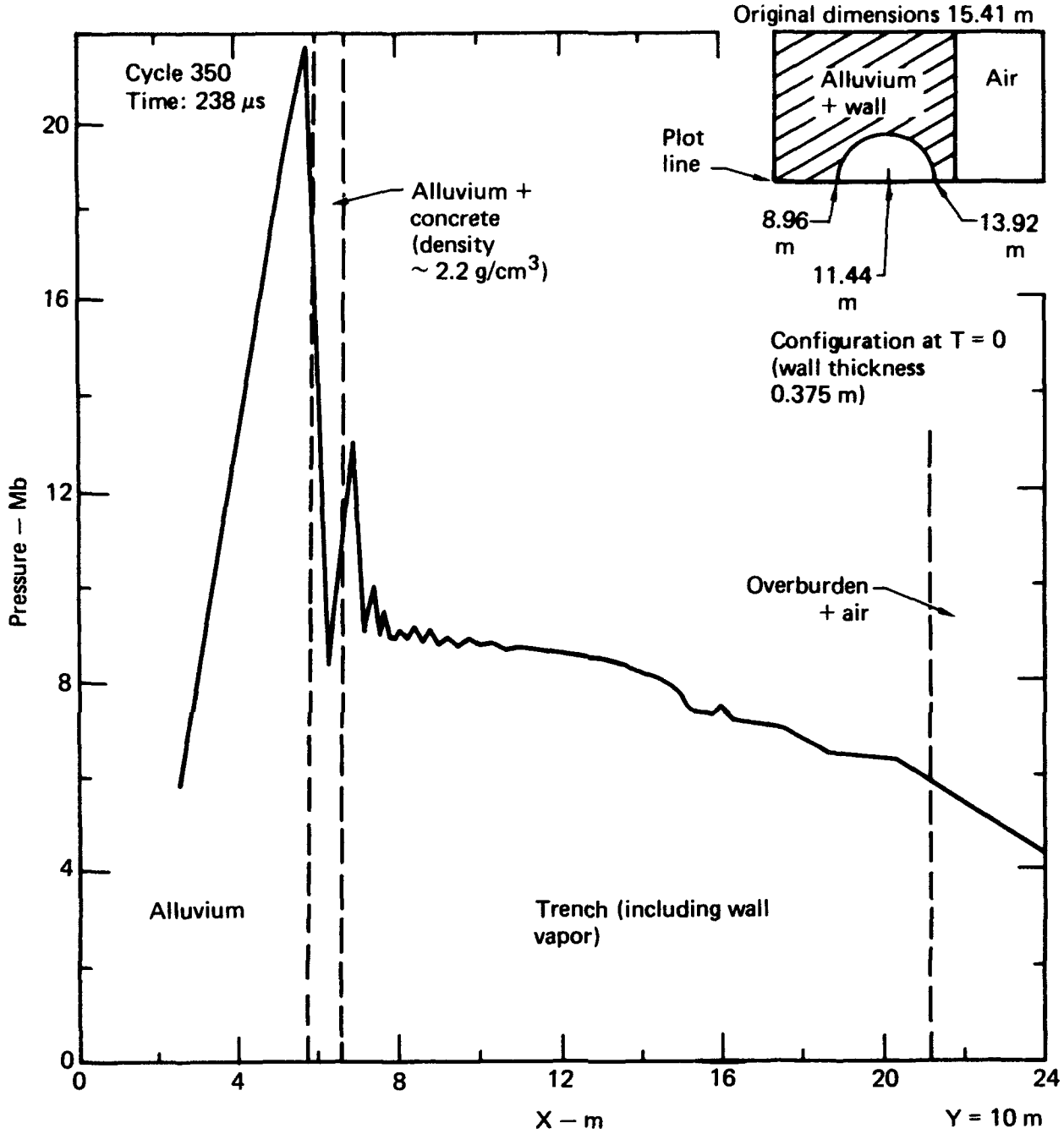

FIG. 19. Pressure profile across tunnel 10 m from source.

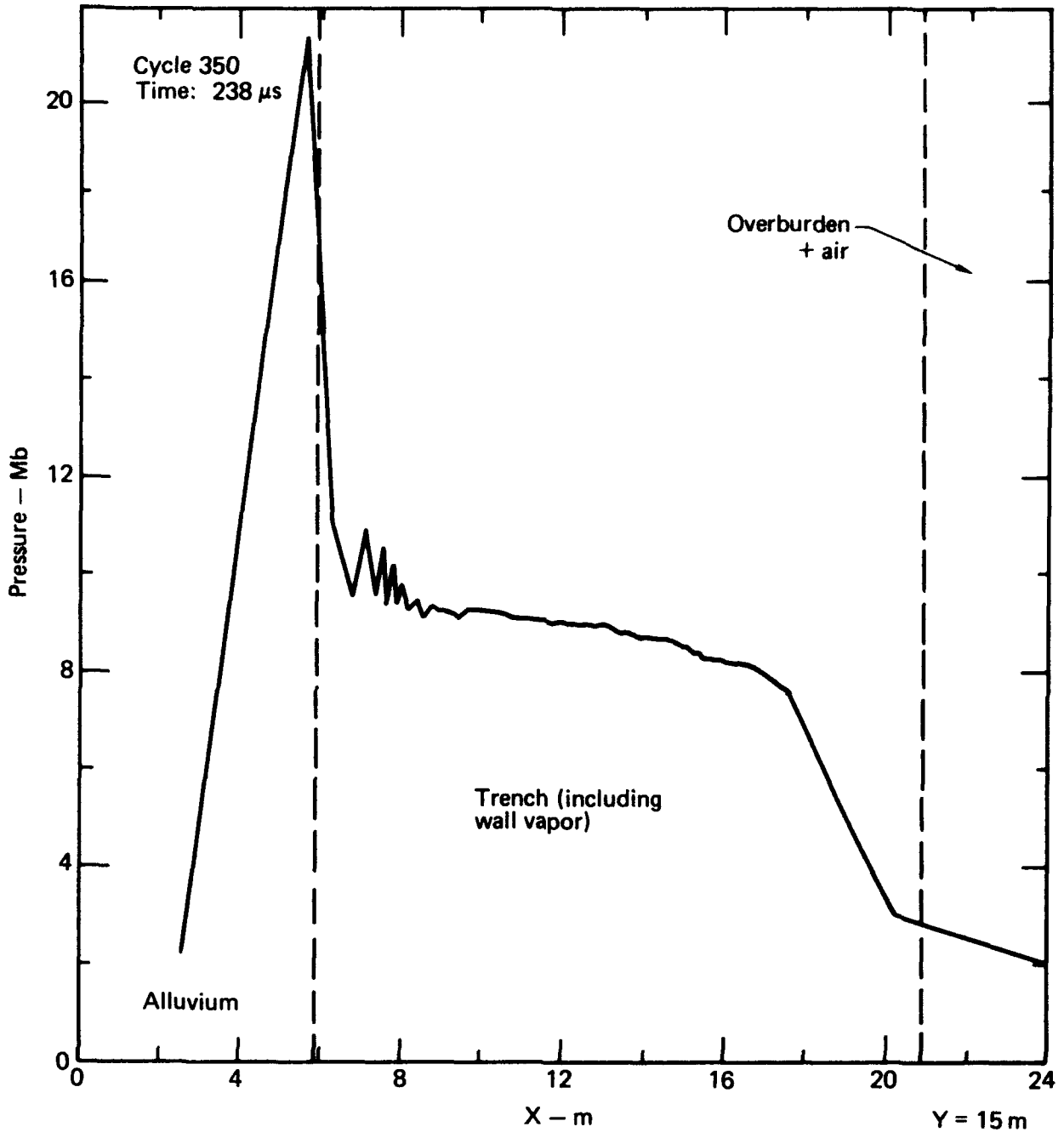

FIG. 20. Pressure profile across tunnel 15 m from source.

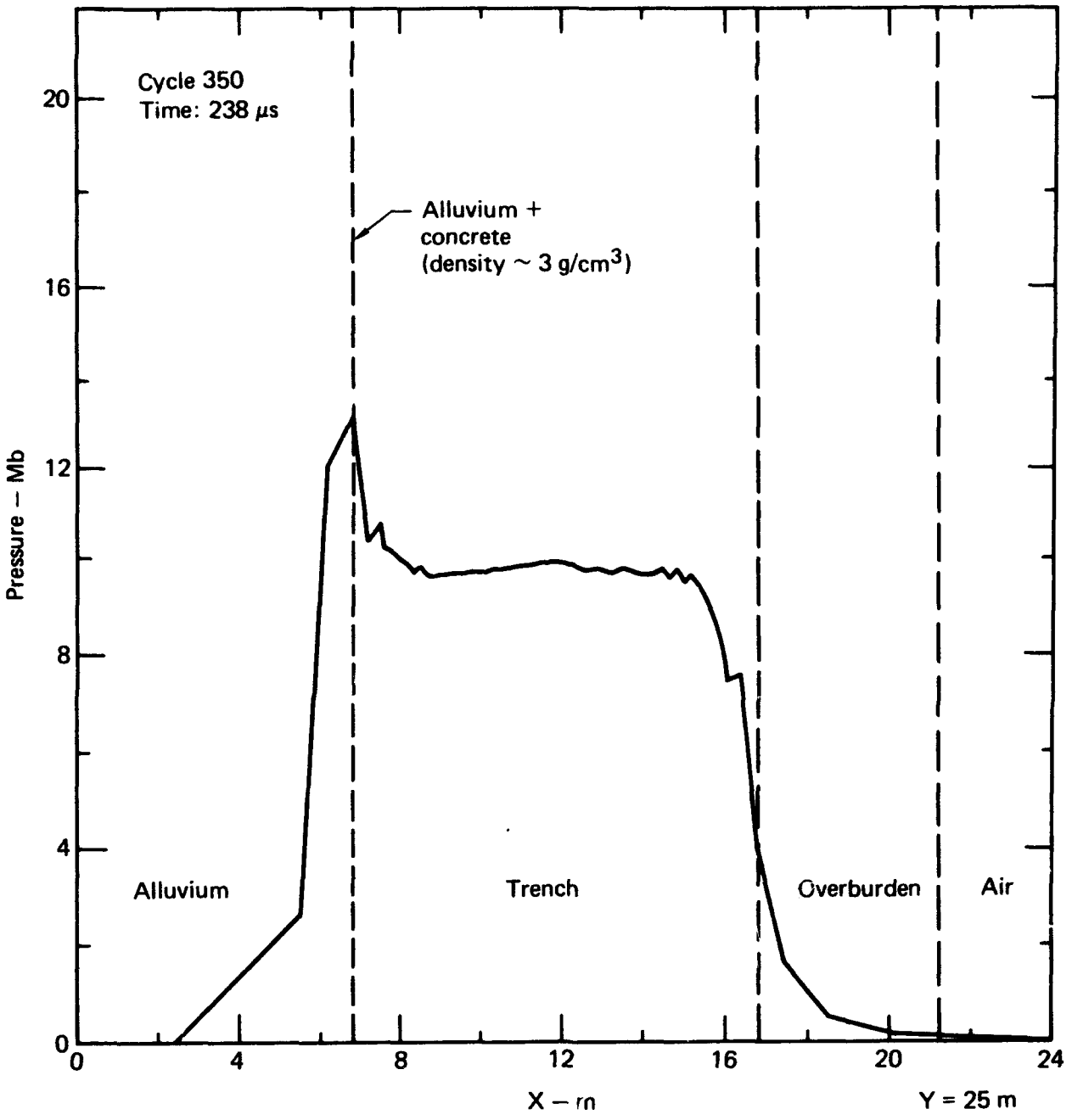

FIG. 21. Pressure profile across tunnel 25 m from source.

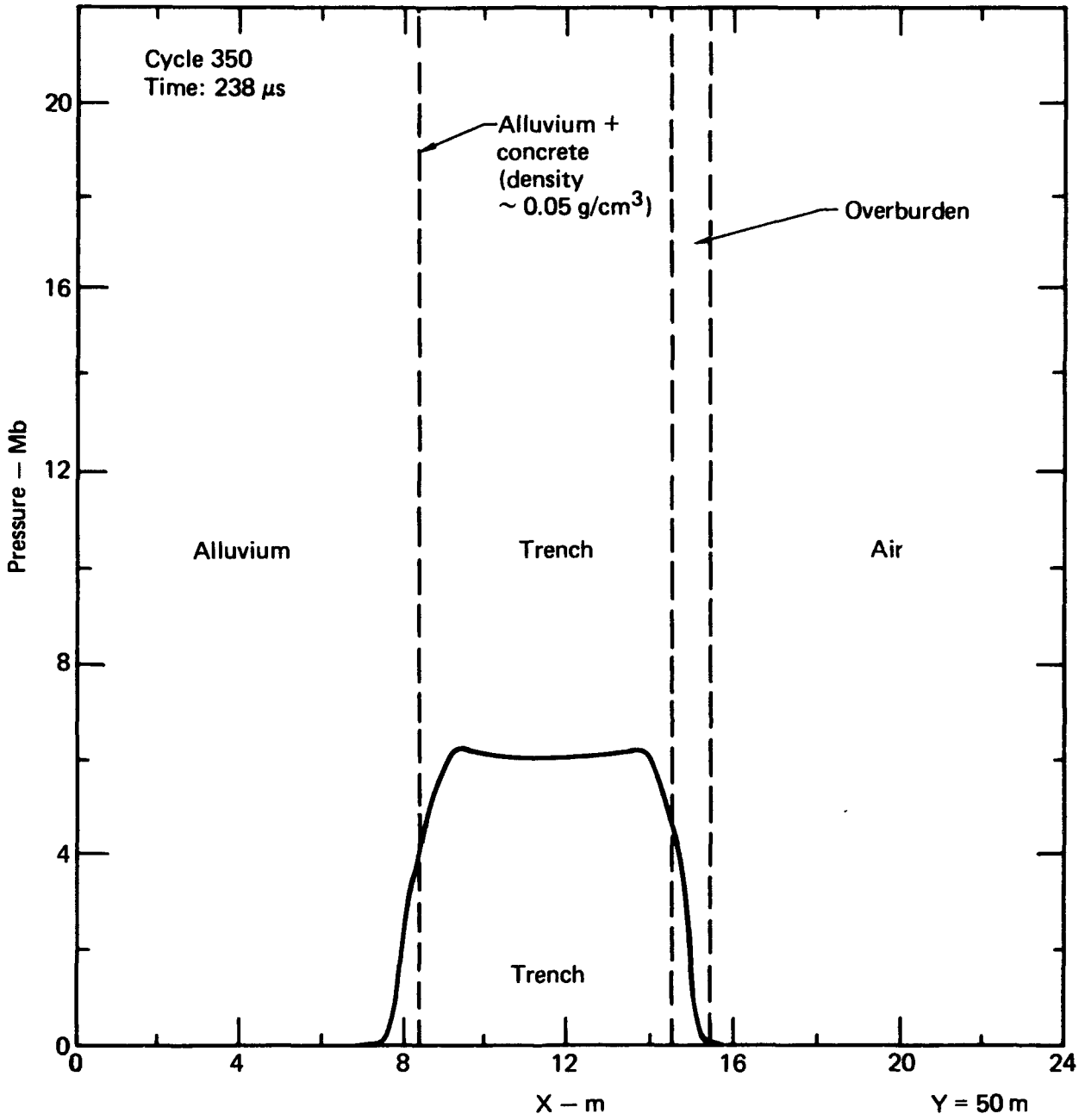

FIG. 22. Pressure profile across tunnel 50 m from source.

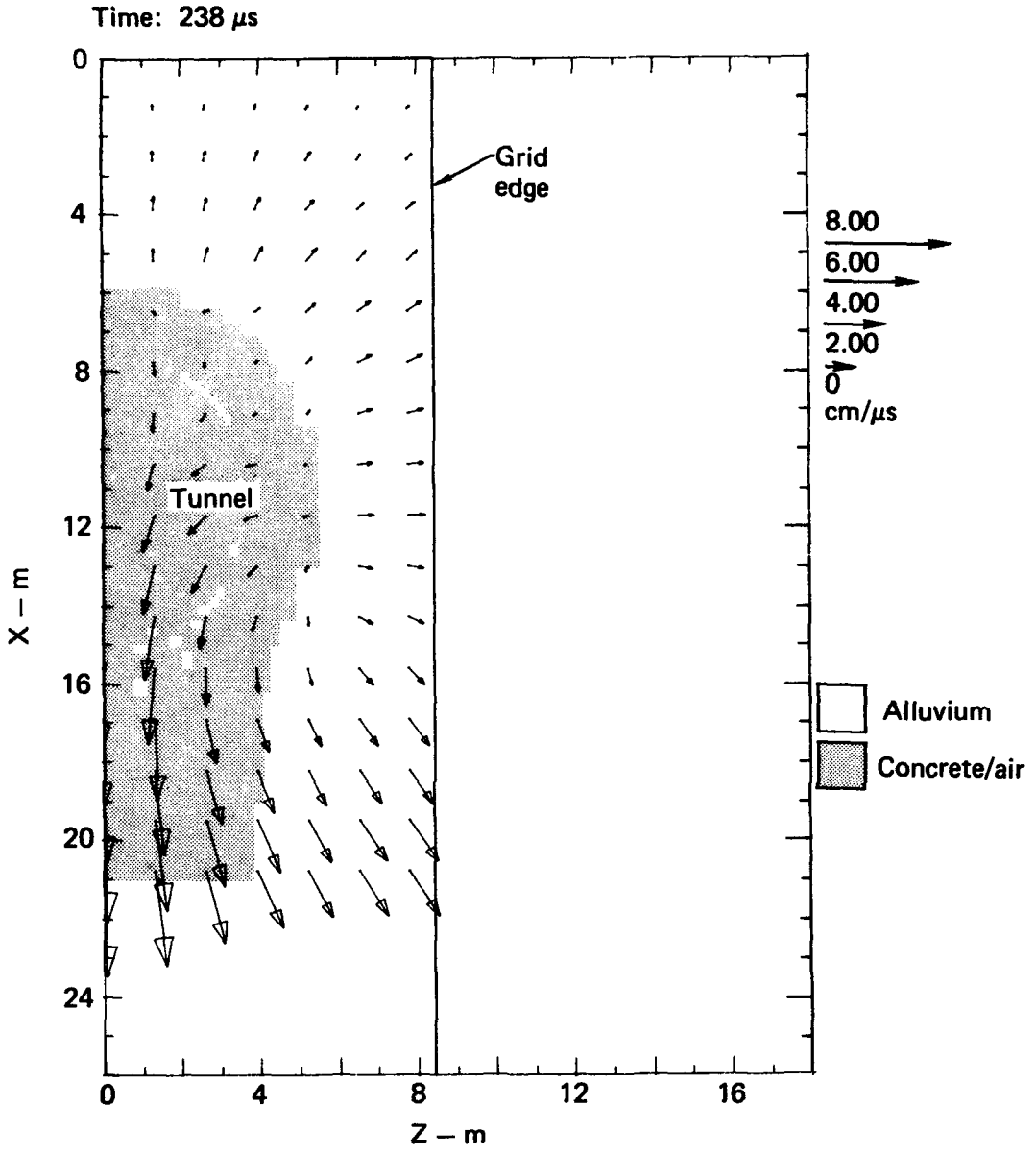

FIG. 23. Material map with velocity vectors 0.7 m from source.

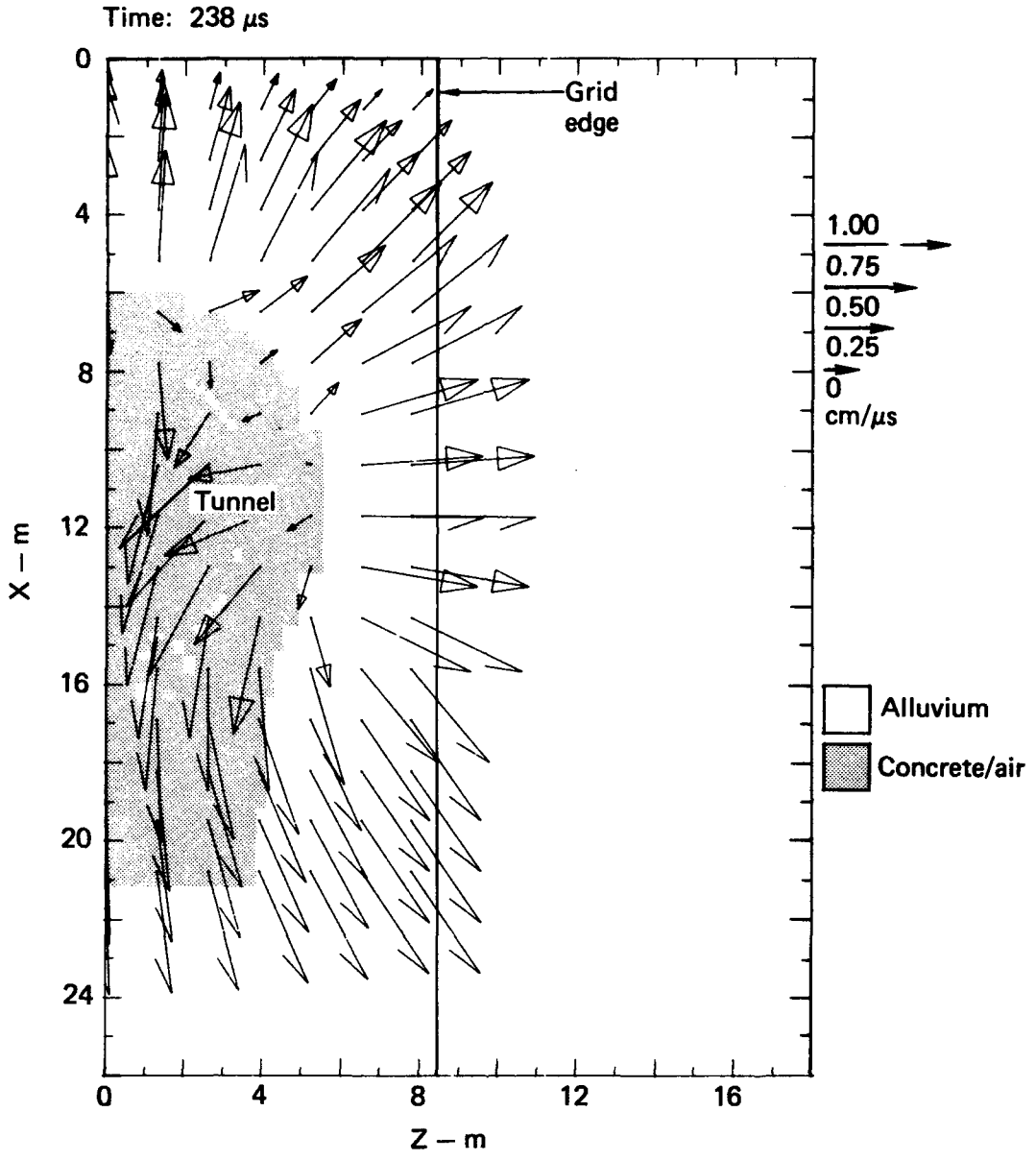

FIG. 24. Material map with exploded velocity vectors 0.7 m from source.

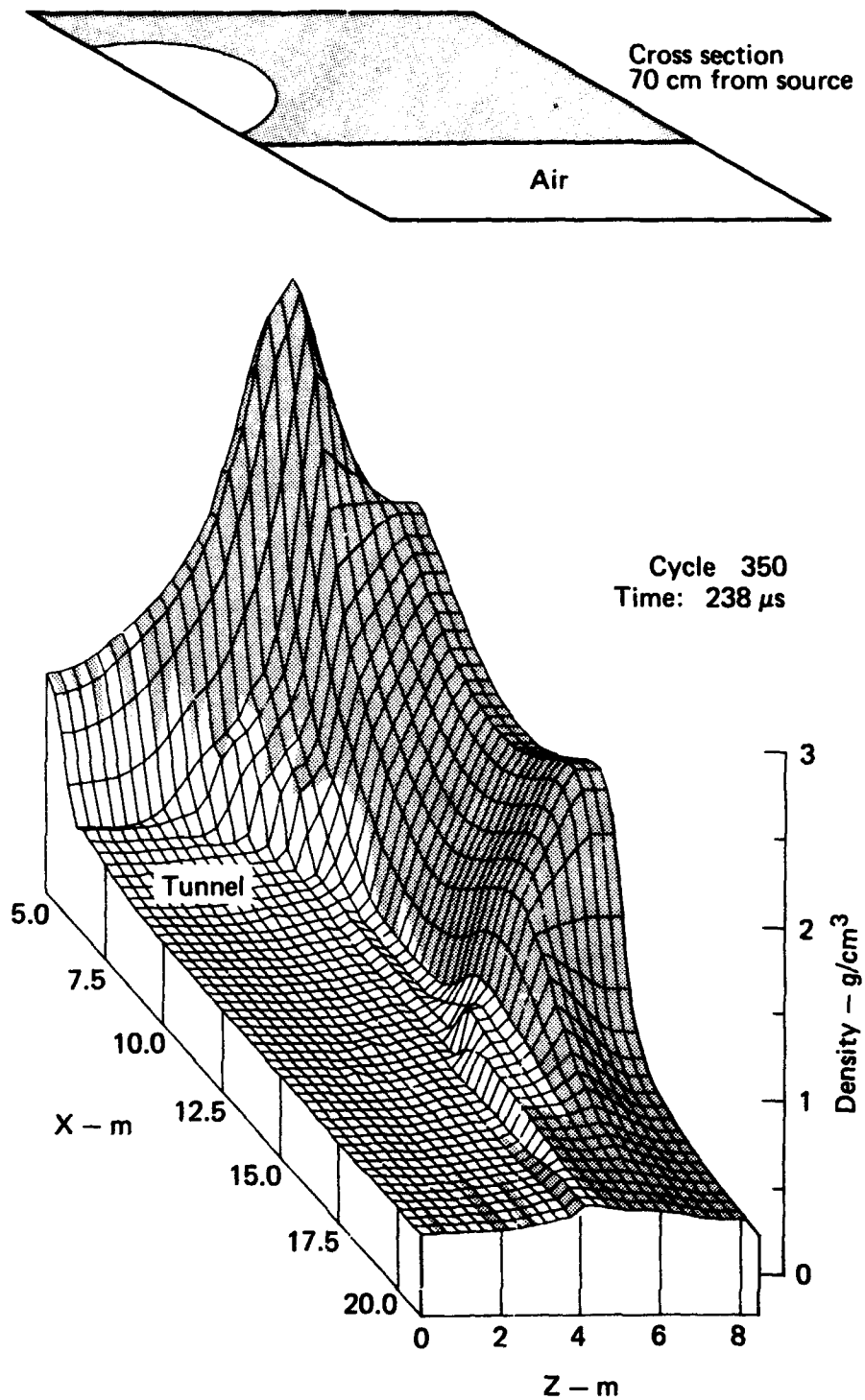

FIG. 25. Isometric density plot 0.7 m from source.

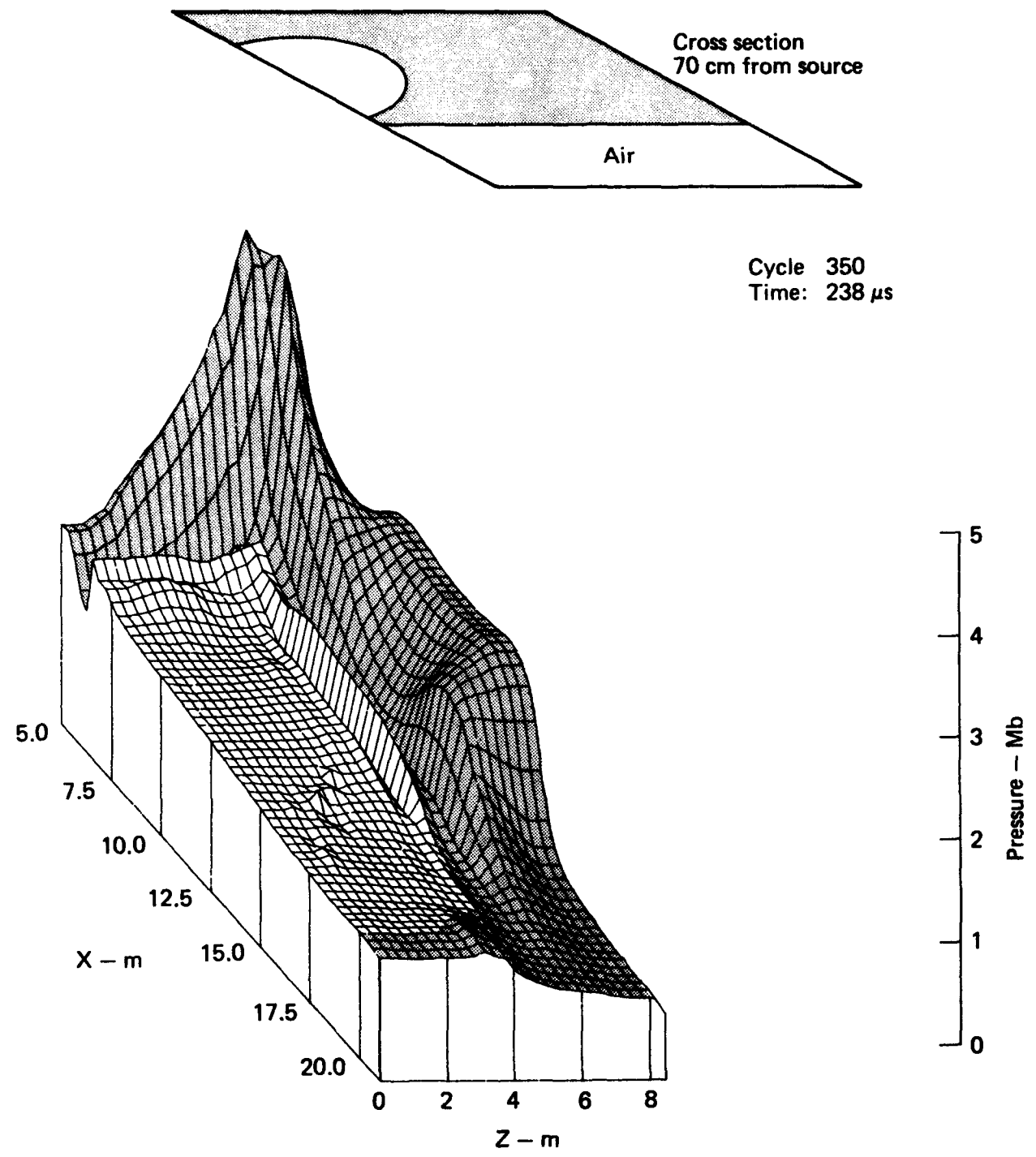

FIG. 26. Isometric pressure plot 0.7 m from source.

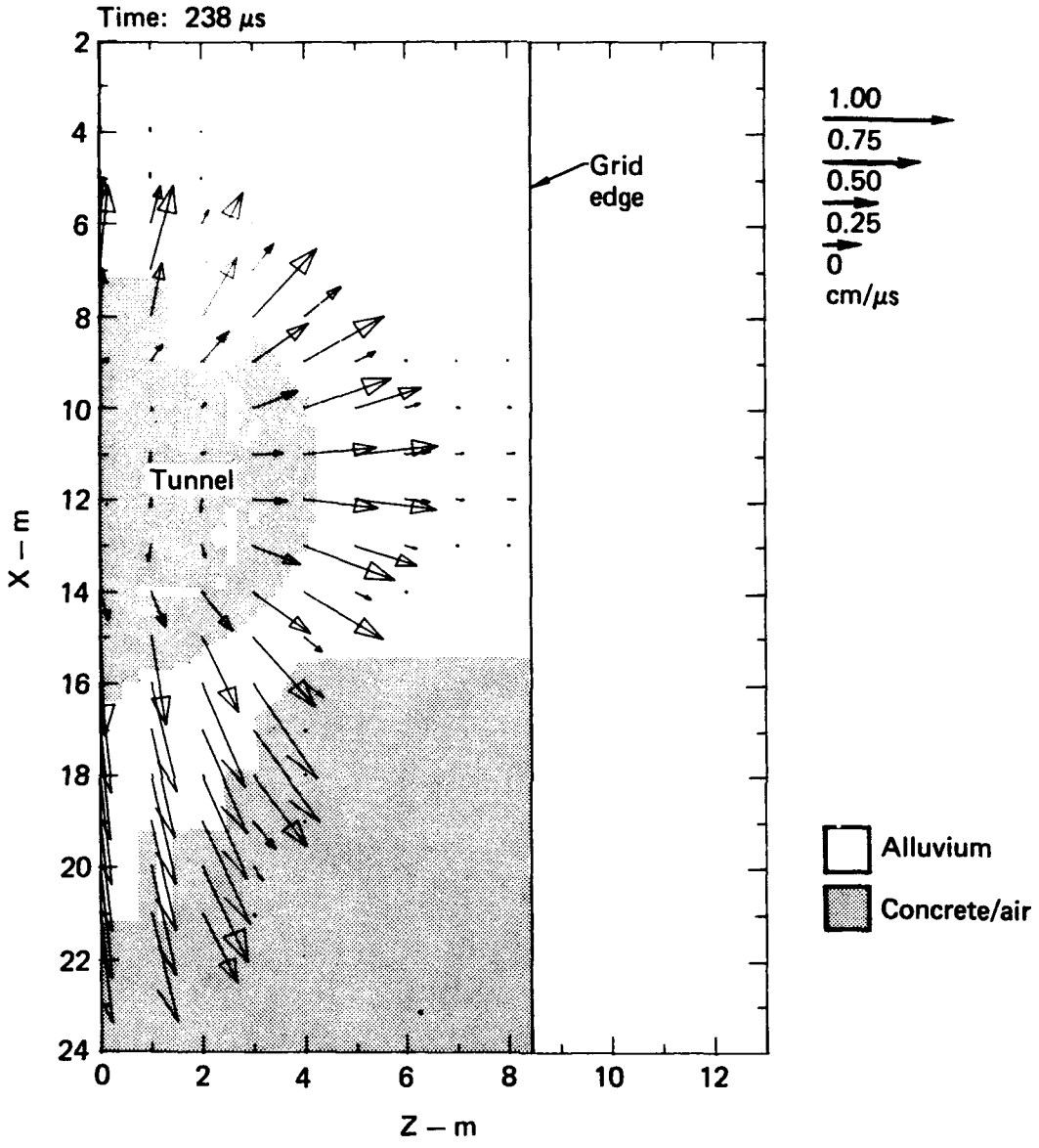

FIG. 27. Material map with velocity vectors 28 m from source.

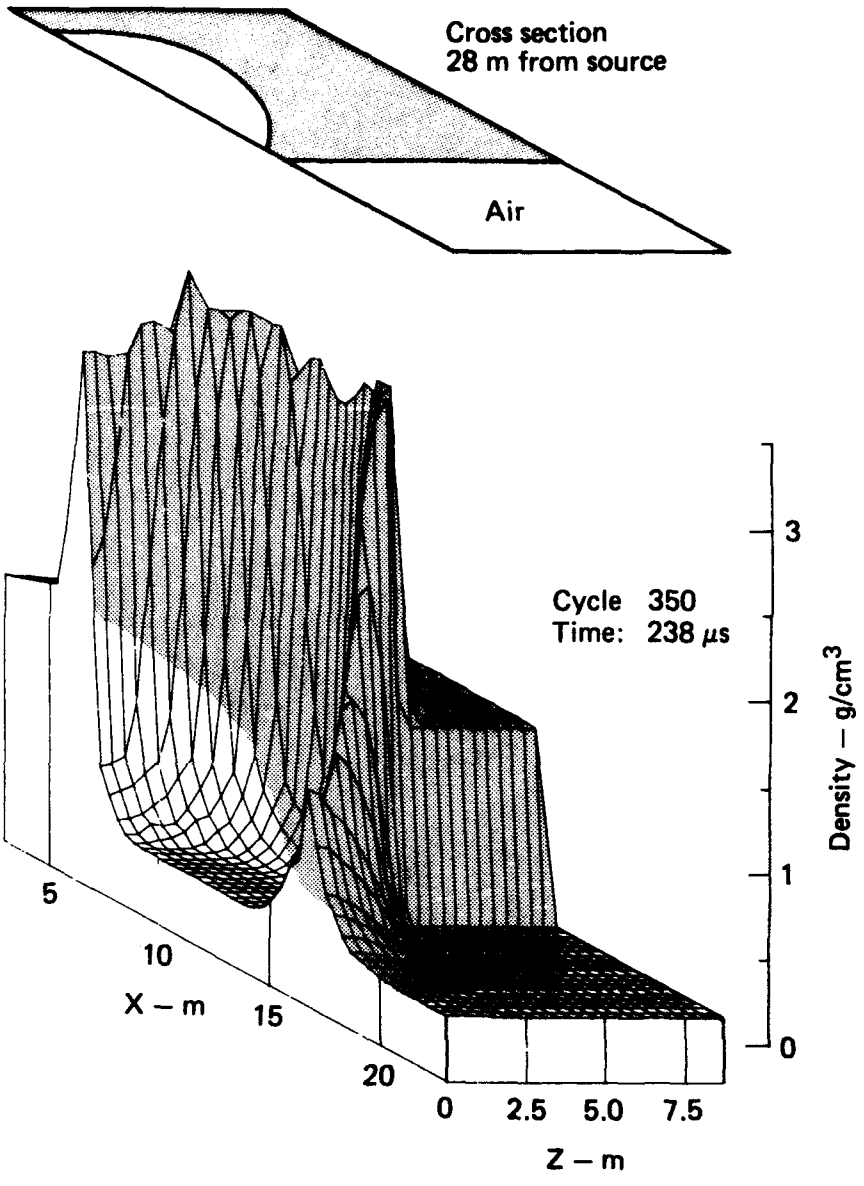

FIG. 28. Isometric density plot 28 m from source.

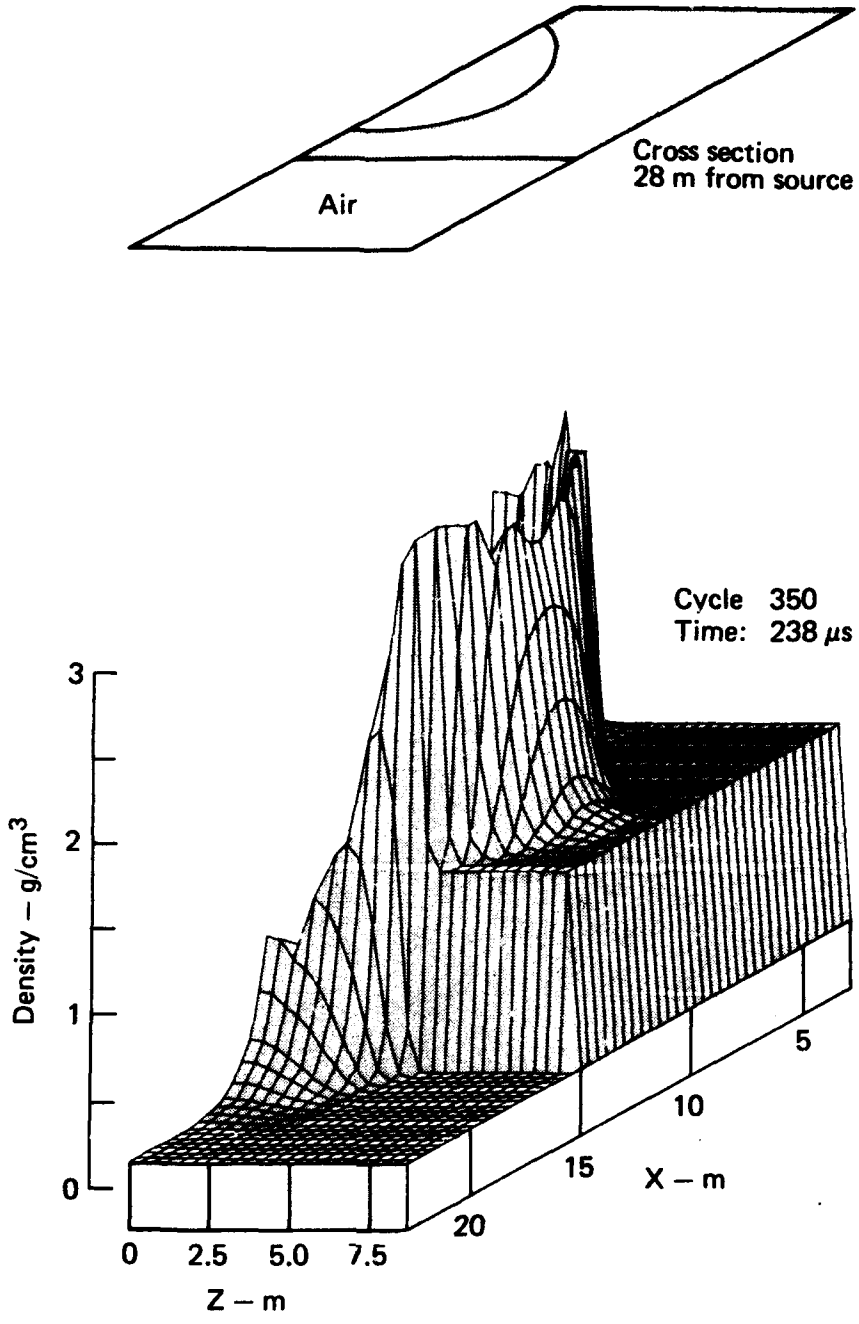

FIG. 29. Isometric density plot 28 m from source.

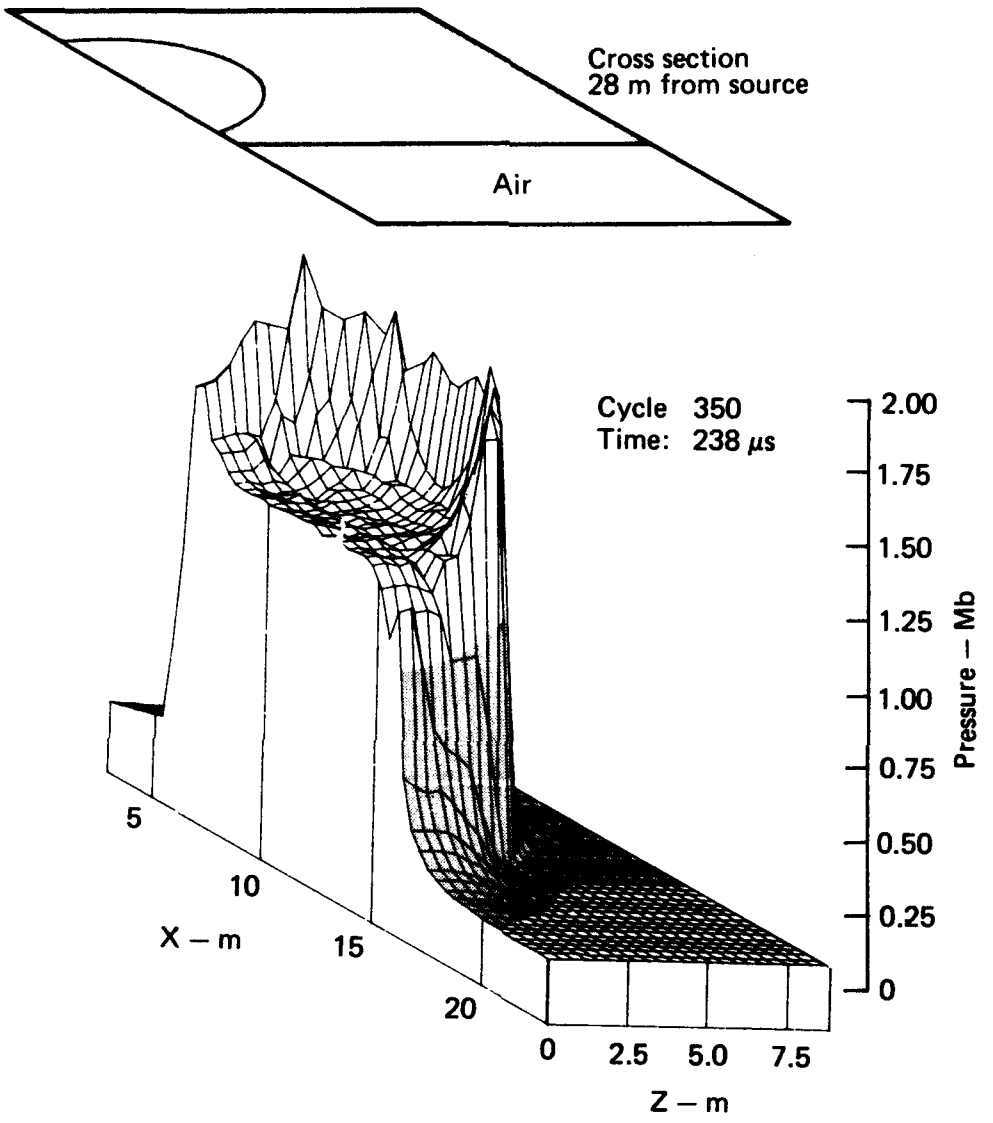

FIG. 30. Isometric pressure plot 28 m from source.

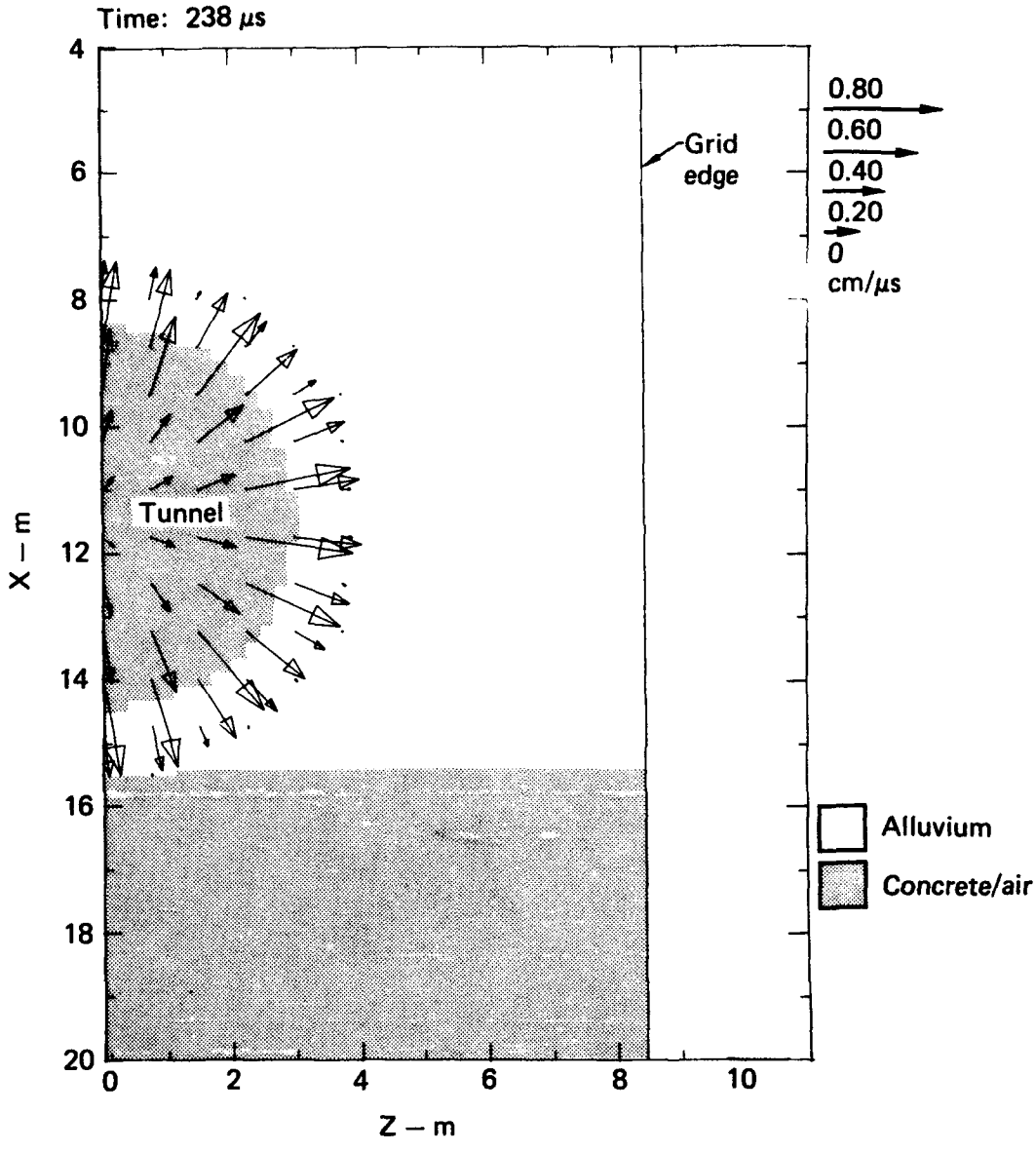

FIG. 31. Material map with velocity vectors 50 m from source.

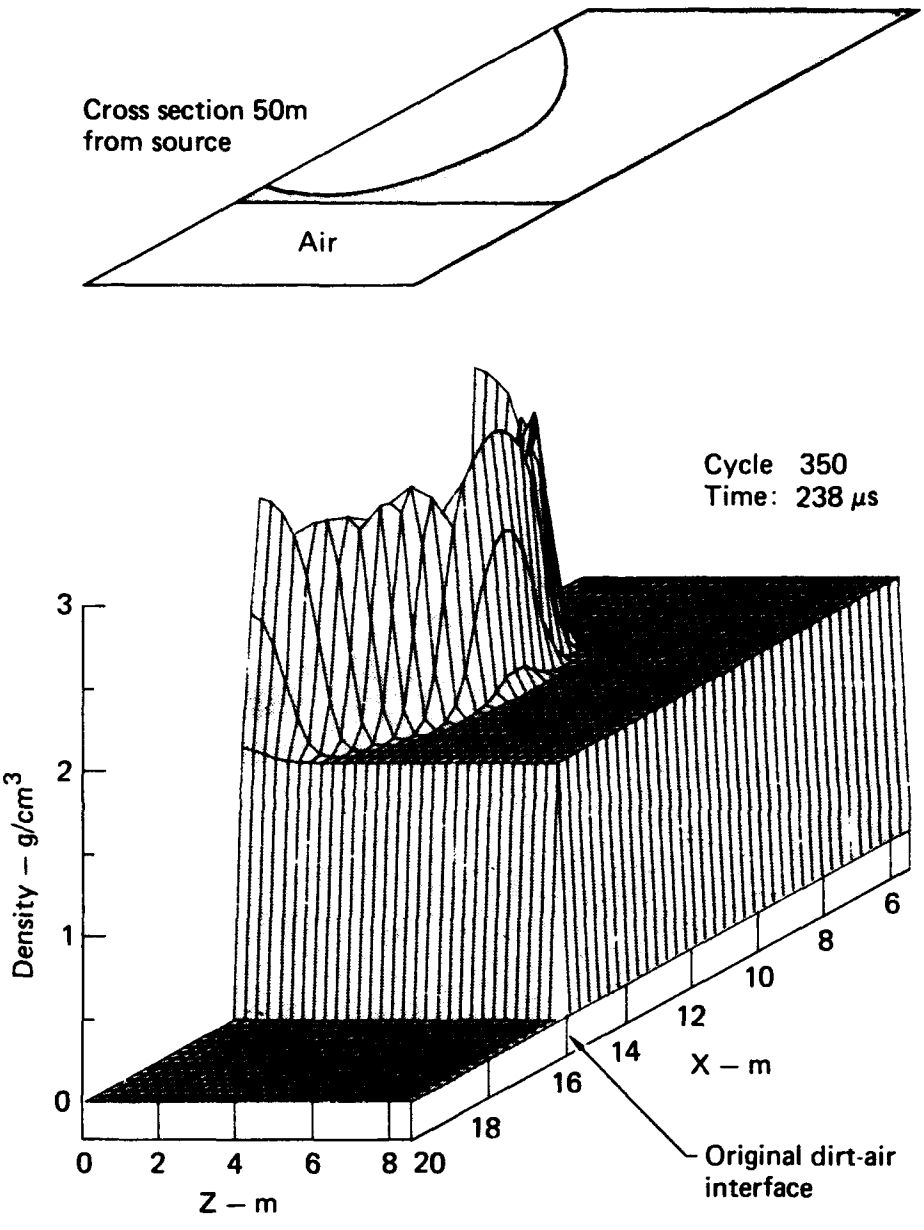

FIG. 32. Isometric density plot 50 m from source.

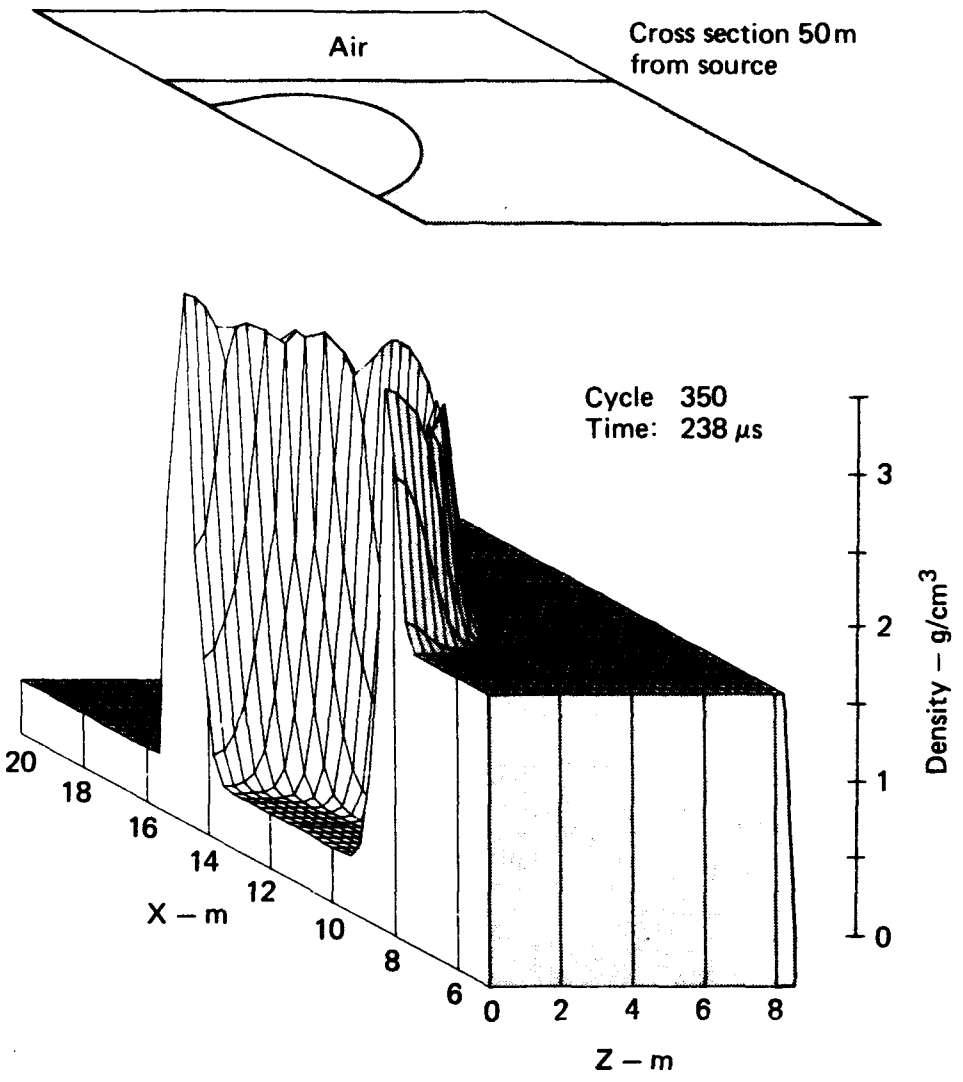

FIG. 33. Isometric density plot 50 m from source.

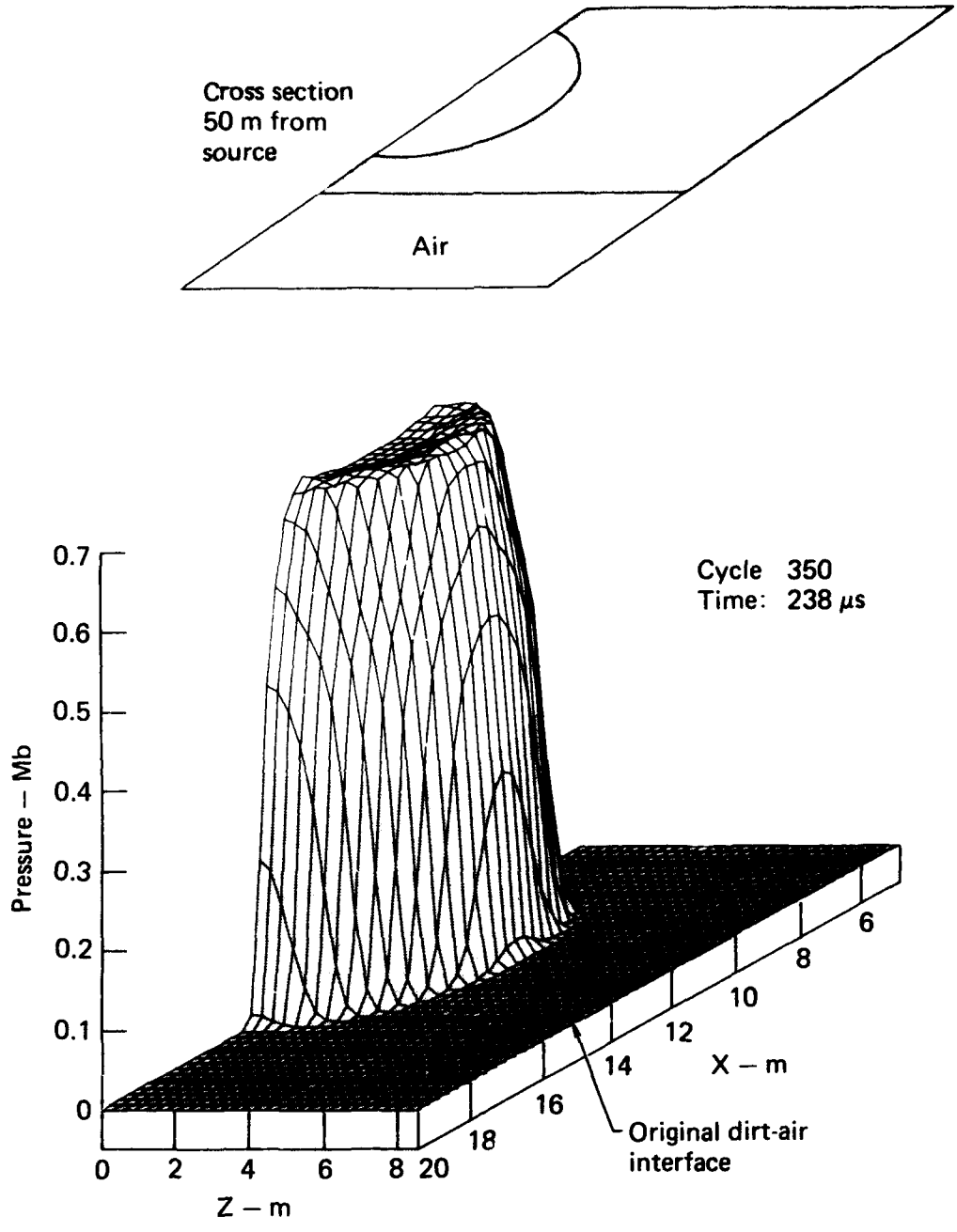

FIG. 34. Isometric pressure plot 50 m from source.

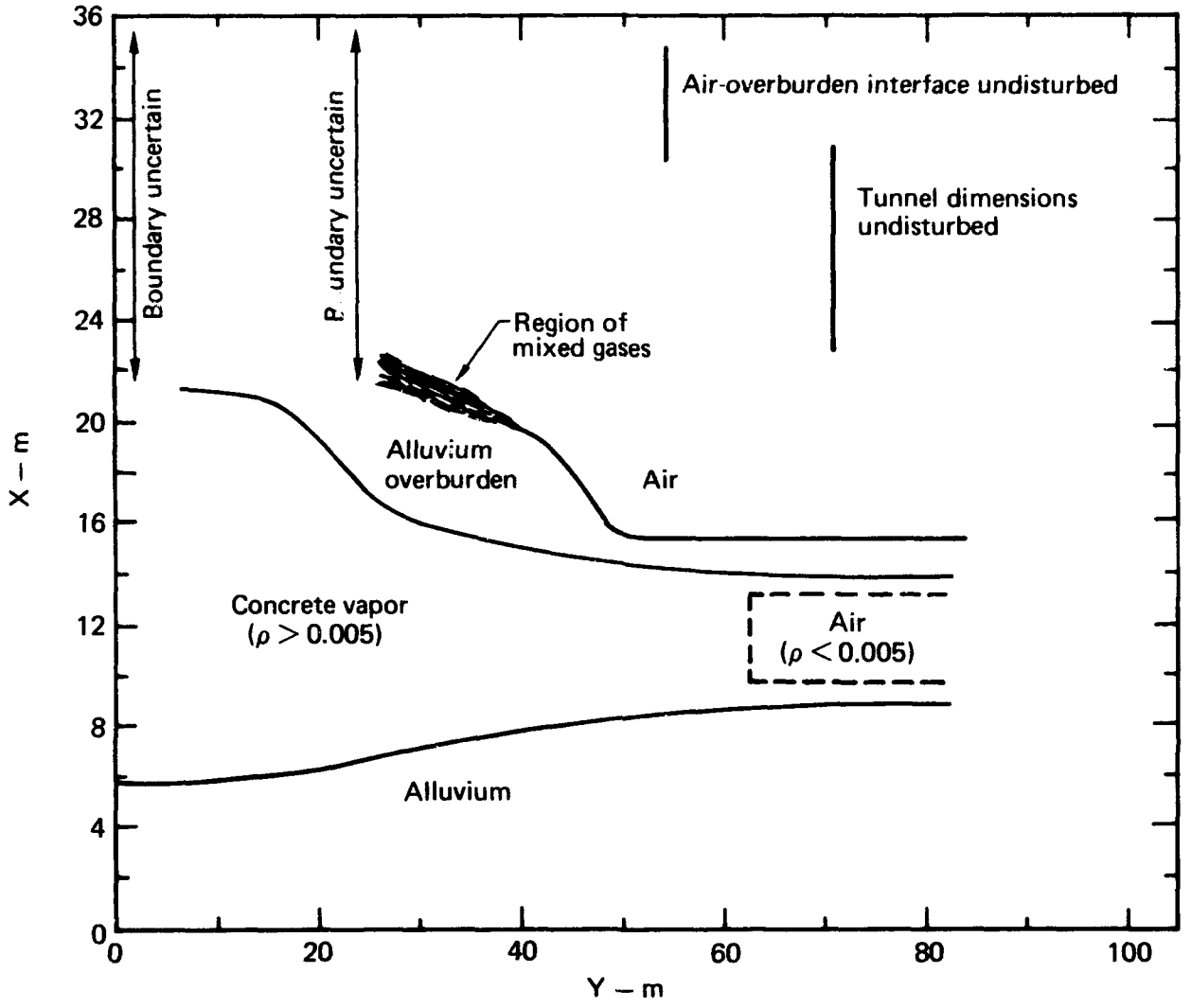

FIG. 35. Geometric configuration on symmetry plane at 238 μs.

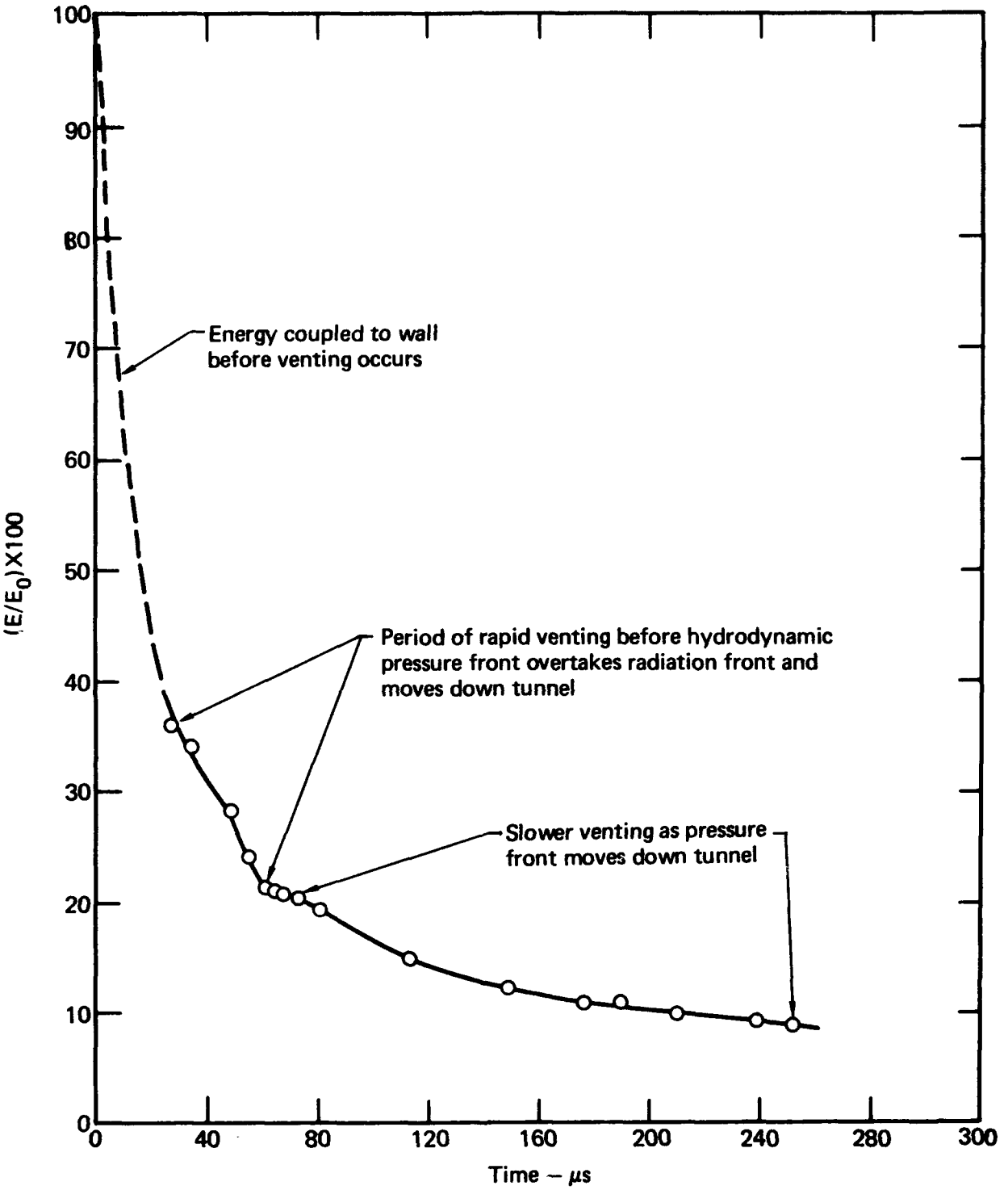

FIG. 36. Fraction of total energy in original tunnel volume as a function of time. Data points are taken at edit times.

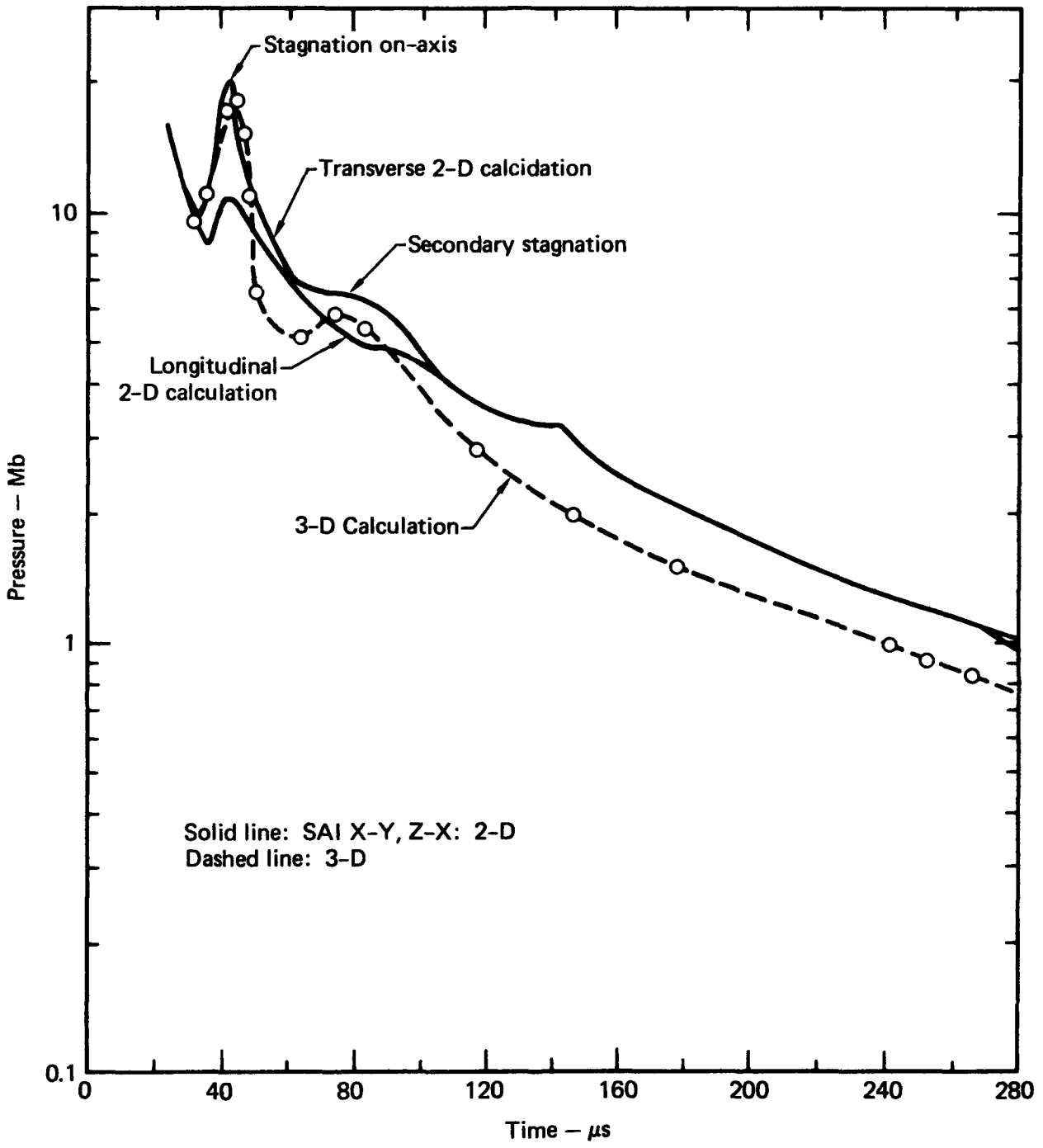

FIG. 37. Peak pressure on tunnel axis as a function of time comparing results of three-dimensional calculations with those of transverse and longitudinal two-dimensional calculations.

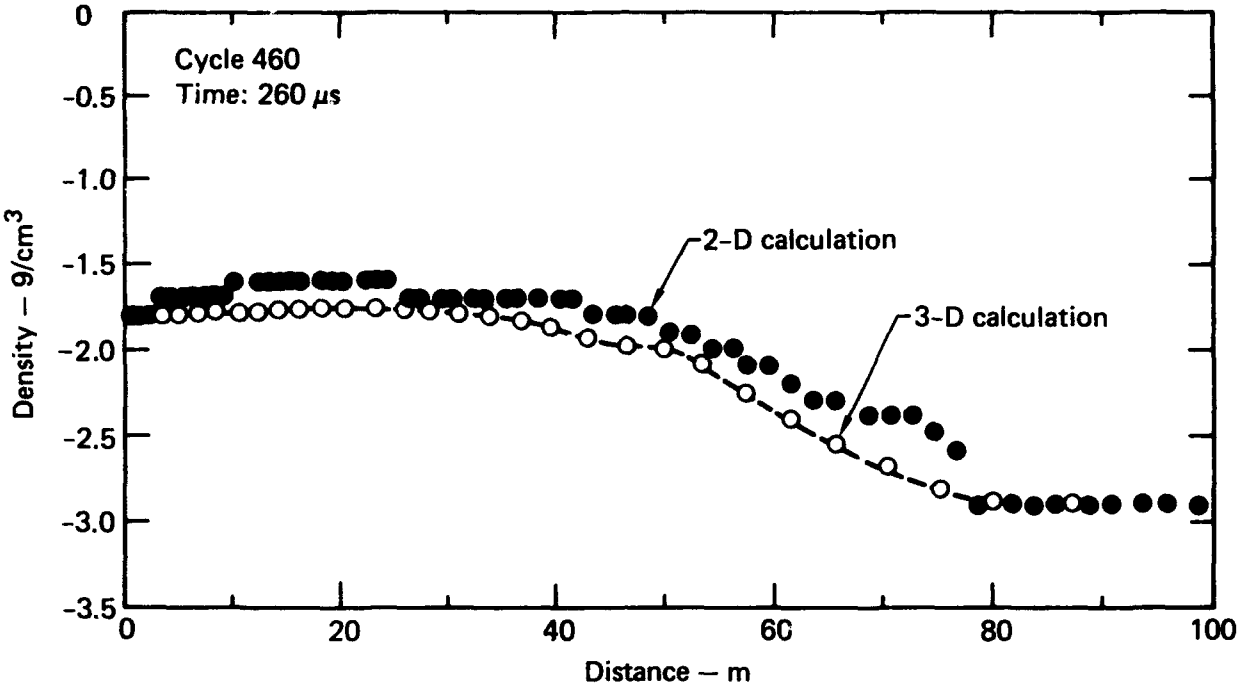

FIG. 38. Comparison of three-dimensional and longitudinal two-dimensional calculations: density.

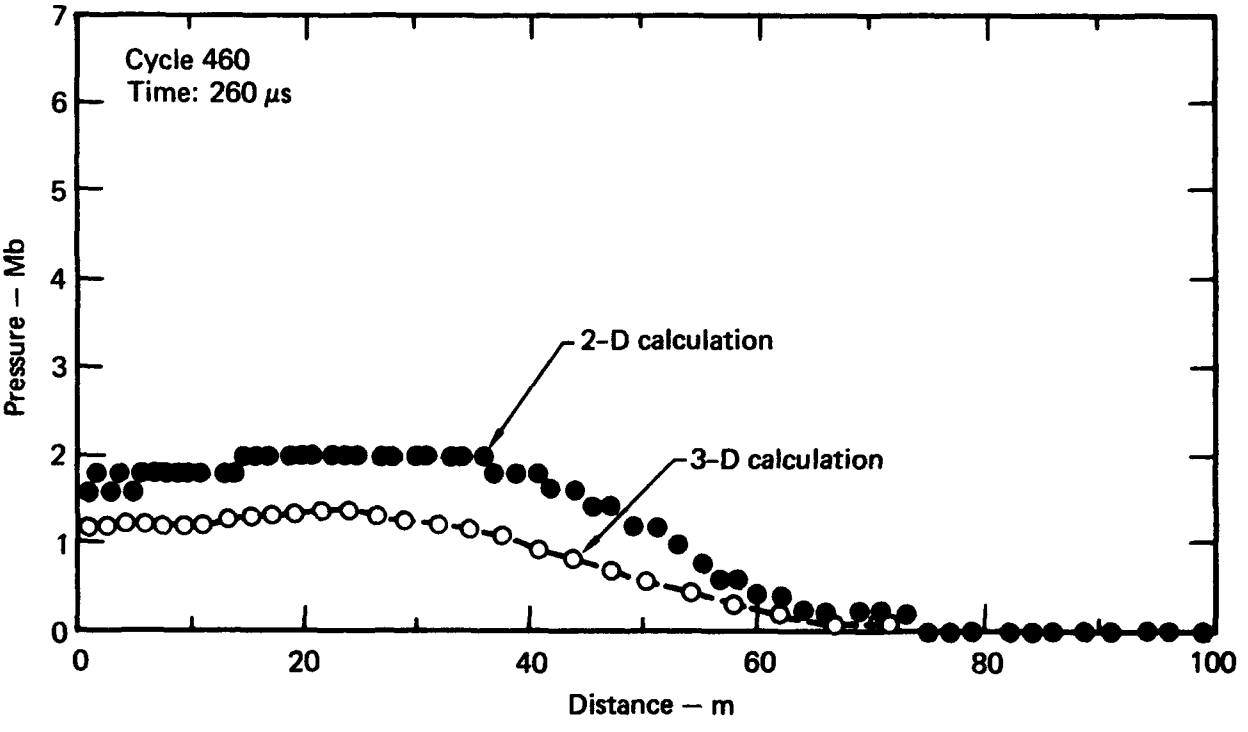

FIG. 39. Comparison of three-dimensional and longitudinal two-dimensional calculations: pressure.

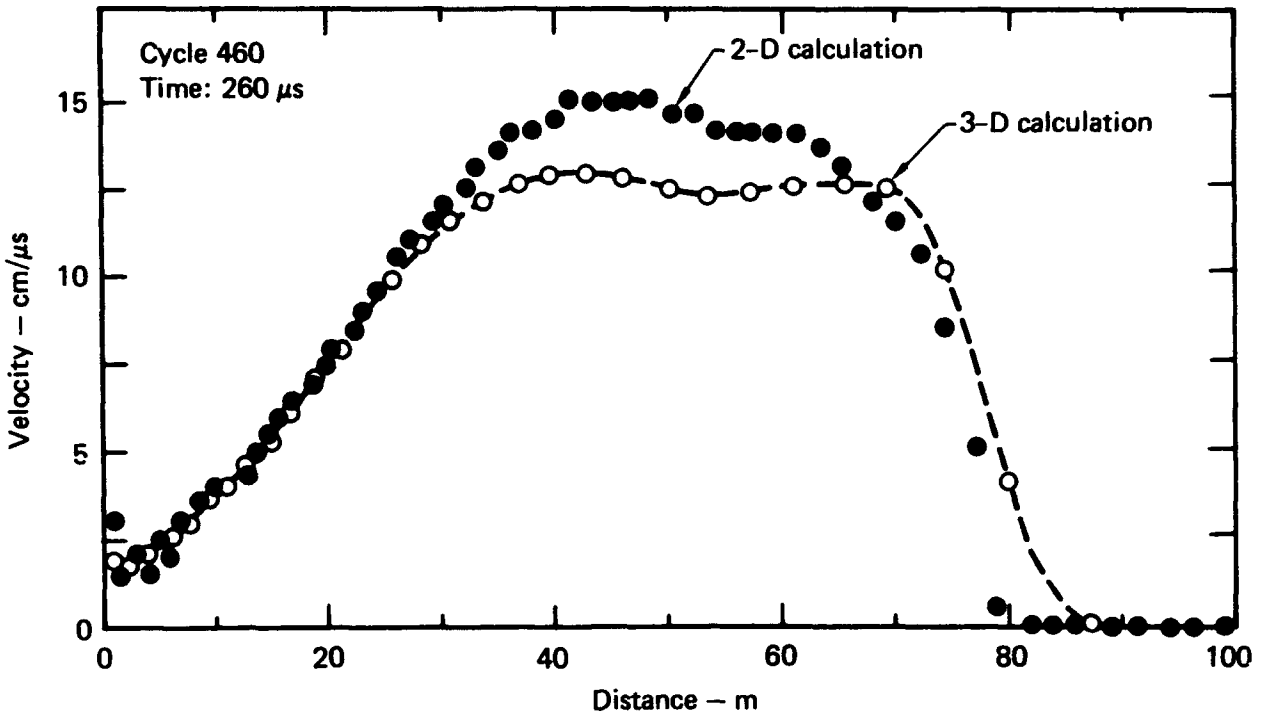

FIG. 40. Comparison of three-dimensional and longitudinal two-dimensional calculations: velocity along tunnel axis.

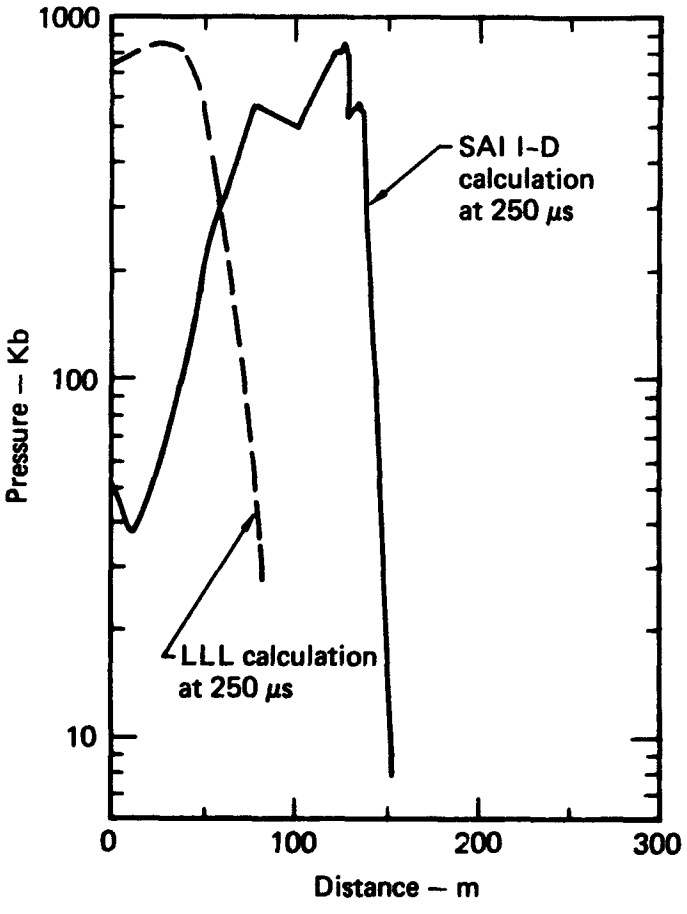

FIG. 41. Comparison of pressure profiles by three-dimensional and one-dimensional calculations at 250 μs.

CONCLUSIONS

The three-dimensional TRIDORF code has been used successfully to calculate the venting that would result from a 1-Mt detonation on-axis in the MX trench. This study demonstrates both the need for and the practicality of using a three-dimensional code for calculations in which the phenomenology of interest is truly three-dimensional. Traditionally it has been argued that one should perform several crude one-dimensional calculations followed by one or two selected two-dimensional calculations and only then, if necessary, by a three-dimensional calculation. Here, however, the phenomenology allows an early-time two-dimensional study but requires a three-dimensional calculation to span the period of venting. At the end of this time, these two calculations can provide satisfactory initial conditions for later 1-1/2- and 2-dimensional studies of the downstream flow.

The three-dimensional calculation was run in a straightforward manner without the need for postulating special models to account for the venting process. The 36,000-zone problem required just 2 h of CDC 7600 computer time.

REFERENCES

1. A. L. Kuhl, *Estimates of Airblast Environments Inside the MX Buried Trench*, TRW Defense and Space Systems Group, Redondo Beach, CA, Report 76.435.9-72 (1976).
2. C. E. Needham and C. Westmoreland, *Airblast Calculations for Advanced Missile Systems (MX Support)*, Air Force Weapons Laboratory, Albuquerque, NM, Report AFWL-TR-75-297 (1976). (Distribution limited to U.S. Government agencies only; AD-B-009 6502, Defense Documentation Center, Alexandria, VA.)
3. R. N. Schlaug and B. F. Chambers III, *Theoretical Calculations in Support of In-Trench Environment Definition for the MX-Concept Validation Phase*, Defense Nuclear Agency, Report DNA-4655F-2, Vol. 2 (1978).
4. W. E. Johnson, *TRIDORF: A Two-Material 3-D Cartesian Hydrodynamics Code Coupled with a Rigid Plastic Strength Model*, Computer Code Consultants, Incorporated, Los Alamos, NM, Report CCC-976 (1976).
5. D. E. Burton and C. M. Snell, *User's Guide to TENPLT (TENSOR Graphics Code) and EOSLIB AND XMUPGENS (Auxiliary Data Codes)*, U. S. Army Engineer Waterways Experimental Station Explosives Evacuation Research Laboratory, Livermore, CA, Miscellaneous Paper E-74-1 (1974).

CSM/ckg

U.S. Government Printing Office: 1980/2 – 689-102/8753